

Angular Distributions and Total Cross Sections of Reactions of Li^6 , Li^7 on B^{10} , $\text{B}^{11}\dagger$

ROBERT L. MCGRATH*

Department of Physics and Astronomy, University of Iowa, Iowa City, Iowa

(Received 3 January 1966)

Charged particles from four sets of reactions induced by Li^6 , Li^7 on B^{10} , B^{11} targets have been observed. The incident beam energy in each case corresponds to 3.05 MeV in the center-of-mass system. A dE/dx , E counter coupled to an on-line computer is used to obtain 115 angular distributions and absolute cross sections of p , d , t , He^3 , and He^4 particles. N^{14} , N^{15} , N^{16} , and C^{13} are formed in several different reactions. The observed relative cross sections are often independent of the mode of formation. Cross sections for low-lying states of these nuclei, and C^{12} , C^{14} are closely proportional to $(2J+1)$ where J is the spin of the residual state. On this basis it is suggested that the statistical compound nucleus mechanism dominates the cross sections to many low-lying states. At high-level excitations, yields typically deviate upwards from $(2J+1)$ dependence. The N^{15} 9.16-MeV and N^{14} 9.13-, 10.09-, and 11.06-MeV states have very large yields in the (Li^6, d) , (Li^7, t) reactions. At these higher excitations direct reactions evidently supplement the statistical yields. Unambiguous evidence for the following unreported levels is found: 7.17 ± 0.04 , 7.37, 8.14, 8.55, 8.93, 9.26, and 9.74 MeV in N^{17} ; 7.66 ± 0.05 , 8.10, 8.36, 8.83, and 9.47 MeV in N^{16} ; and 10.79 ± 0.03 MeV in N^{14} (previously reported as 10.71 ± 0.09 MeV).

I. INTRODUCTION

NUCLEAR interactions induced by low-energy (several MeV) lithium ions on light targets are of interest for several reasons. The Q values of such reactions are usually large for a number of exit channels, allowing the formation of many residual levels. Further, the cluster structure¹ of Li^6 and Li^7 may permit spectroscopic studies of bound alpha, deuteron, or triton cluster states. Such alpha states are relatively inaccessible to reactions induced by lighter projectiles. Reactions which involve only the rearrangement of clusters in the initial and final nuclei are expected to have enhanced cross sections and to exhibit characteristic direct-reaction angular distributions.² The inverse (d, Li^6) reaction at 15 MeV, an energy considerably larger than the incident Coulomb barrier, has provided evidence for alpha clustering in the ground states of several light nuclei.³

Most work on lithium-induced reactions has been carried out at energies from 1 to 4 MeV on targets ranging from $A=6$ to 12.⁴ The Coulomb barrier varies from 4.8 to 6.3 MeV. It is anticipated that such reactions will be complicated by large Coulomb and nuclear distortions and perhaps by contributions from both direct and compound nucleus mechanisms. Angular distributions of the $\text{Be}^9(\text{Li}^6, \alpha)\text{B}^{11}$ reactions have been

shown to be asymmetric (however, yields in the backward and forward directions are comparable) and to have little dependence on incident energy between 2 and 4 MeV.⁵ Similar studies on $\text{Li}^6 + \text{C}^{12}$ reveal differential-cross-section fluctuations in proton and deuteron channels at the higher energies which are attributed to states of the compound nucleus F^{18} .^{6,7} The alpha particle channels again show little energy dependence. At 2 MeV, negligible yields to the B^{10} 1.74 MeV level ($J\pi=0^+$, $T=1$) compared to other levels in both the $\text{Li}^6(\text{Li}^6, d)$, and $\text{Li}^6(\text{Li}^6, t)$ reactions have been interpreted as evidence of direct alpha transfer.⁸

The present experiment is intended to elucidate the dominant (if any) reaction mechanisms in proton, deuteron, triton (and He^3), and alpha particle reactions in the $\text{Li}^6 + \text{B}^{10}$, $\text{Li}^7 + \text{B}^{10}$, $\text{Li}^6 + \text{B}^{11}$, and $\text{Li}^7 + \text{B}^{11}$ systems. Over 100 angular distributions and absolute total cross sections of the reactions listed in Table I have been measured. The incident energies vary between 4.72 and 5.20 MeV, fixing the incident center-of-mass energy at 3.05 MeV. The Coulomb barrier is approximately 3.57 MeV ($r_0=1.5$ F) in all cases. Consequently, the incident Coulomb penetrabilities are equal for all reactions if the effects of slight radius changes are ignored.

The momentum transfers, and initial and final kinetic energies, are almost equal in the (Li^6, d) and (Li^7, t) reactions. It has been suggested⁹ that if alpha transfer is important, then the relative cross reactions for these two reactions ought to be similar. In plane-wave Born approximation, the (d, p) stripping amplitude is proportional to the neutron reduced width factor times an integral that depends in part on momentum transfers

[†] Research supported in part by National Science Foundation.

* Present address: Lawrence Radiation Laboratory, Berkeley, California.

¹ C. Ruhla, M. Riou, J. P. Garron, J. C. Jacmart, and L. Massonnet, *Phys. Letters* **2**, 44 (1962); H. G. Pugh, *Bull. Am. Phys. Soc.* **10**, 1091 (1965).

² G. C. Phillips, *Direct Interactions and Nuclear Reaction Mechanisms* (Gordon and Breach Science Publishers, Inc., New York, 1963), p. 869.

³ W. W. Daehnick and L. J. Denes, *Phys. Rev.* **136**, B1326 (1964); R. M. Drisko, G. R. Satchler, and R. H. Bassel, in *Proceedings of the 3rd International Conference on Reactions Between Complex Nuclei, 1963* (University of California Press, Berkeley, California, 1963), p. 85.

⁴ A survey is given by G. C. Morrison, *Direct Interactions and Nuclear Reaction Mechanisms* (Gordon and Breach Science Publishers, Inc., New York, 1963), p. 878.

⁵ J. J. Leigh and J. M. Blair, *Phys. Rev.* **121**, 246 (1961).

⁶ J. M. Blair and R. K. Hobbie, *Phys. Rev.* **128**, 2282 (1962).

⁷ D. W. Heikkinen, *Phys. Rev.* **141**, 1007 (1966).

⁸ G. C. Morrison, *Phys. Rev. Letters* **5**, 565 (1960).

⁹ G. C. Morrison, N. H. Gale, and M. Hussain, in *Proceedings of the 3rd International Conference on Reactions Between Complex Nuclei, 1963* (University of California Press, Berkeley, California, 1963), p. 168.

and the orbital angular momentum of the captured neutron. If the cluster-model assumption is made for the lithium nuclei, and an analogy is made to (d, p) stripping, then the (Li^6, d), (Li^7, t) cross sections are expected to be similar. It is also suggested⁹ that these results would hold in a distorted-wave calculation to the extent that both Li^6 and Li^7 , and d and t scattering states are equivalent. Unfortunately, the p -wave nature of the ($\alpha+t$) Li^7 cluster configuration allows a different set of possible angular momentum transfers compared to the s -wave ($\alpha+d$) Li^6 structure. Consider the $\text{B}^{10}(\text{Li}^6, d)\text{N}^{14}$ and $\text{B}^{10}(\text{Li}^7, t)\text{N}^{14}$ reactions leading to the 6.44-MeV 3^+ level. The allowed angular momentum transfers are 0, 2, 4, and 6 in the former reaction. In the latter, since there is no longer a connection between the angular momentum transfer and the parity of the transition,¹⁰ transfers of 1, 2, 3, 4, 5, 6, and 7 are permitted. Similarly, the same reactions leading to 1^+ levels allow 2, 4 and 1, 2, 3, 4, 5 angular momentum transfers, respectively.

These examples are typical; the (Li^7, t) reactions have a larger set of allowed angular momentum transfers. Thus it should be expected that the relative total cross sections for the two reactions are similar (because of the proportionality to the alpha particle reduced width), but that the differential cross sections may be different even where alpha transfer accounts for most of the yield.

On the other hand, if compound nucleus formation is important in these reactions, then the statistical theory should be applicable. The excitation energies of the compound nuclei O^{16} , O^{17} , and O^{18} range from 27 to 34 MeV. Using the continuum theory,¹¹ one finds that partial waves up to $L=5\hbar$ contribute significantly to the cross sections; the incoming channel spins are quite large. Therefore population of a large fraction of the compound states contained in the energy interval corresponding to the experimental resolution should be possible. In this picture, the relative cross sections of residual states produced in the sets of reactions from $\text{Li}^7+\text{B}^{10}$ and $\text{Li}^6+\text{B}^{11}$ should be almost equal since the yields are primarily dependent on penetrability and phase-space factors in the compound nucleus decay process from O^{17} at similar excitation energies. The statistical theory also predicts angular distribution symmetry, and under certain conditions¹² that yields are proportional to $(2J+1)$ where J is the final-state spin. Fluctuations about the averages given by the statistical theory are determined by sizes of the compound nucleus level widths, spacings, and the experimental energy resolution.¹³ These parameters are estimated below.

The rather large collection of data from the reactions given in Table I refer to four nitrogen and three carbon

TABLE I. Reactions observed in the present experiment.

$\text{Li}^6+\text{B}^{10}$ ($E_{\text{Li}^6}=4.89$ MeV) \rightarrow	O^{16}	+30.85 MeV
	$\text{N}^{16}+p$	+18.74
	$\text{N}^{14}+d$	+10.14
	$\text{N}^{13}+t$	+ 5.85
	$\text{C}^{13}+\text{He}^3$	+ 8.09
	$\text{C}^{12}+\alpha$	+23.70
$\text{Li}^7+\text{B}^{10}$ ($E_{\text{Li}^7}=5.20$ MeV) \rightarrow	O^{17}	+27.75 MeV
	$\text{N}^{16}+p$	+13.99
	$\text{N}^{15}+d$	+13.72
	$\text{N}^{14}+t$	+ 9.15
	$\text{C}^{13}+\alpha$	+21.41
$\text{Li}^6+\text{B}^{11}$ ($E_{\text{Li}^6}=4.72$ MeV) \rightarrow	O^{17}	+23.54 MeV
	$\text{N}^{16}+p$	+ 9.78
	$\text{N}^{15}+d$	+ 9.51
	$\text{N}^{14}+t$	+ 4.93
	$\text{C}^{13}+\alpha$	+17.19
$\text{Li}^7+\text{B}^{11}$ ($E_{\text{Li}^7}=5.00$ MeV) \rightarrow	O^{18}	+24.36 MeV
	$\text{N}^{17}+p$	+ 8.42
	$\text{N}^{16}+d$	+ 4.76
	$\text{N}^{15}+t$	+ 8.52
	$\text{C}^{14}+\alpha$	+18.12

isotopes. The states of four residual nuclei are observed by at least three different means; thus comparisons of cross sections (and perhaps angular distributions) can lead to conclusions about the reaction mechanisms. Indeed a motivation for this experiment results from the observed similarities in gamma-ray spectra from $\text{Li}^7+\text{B}^{10}$ and $\text{Li}^6+\text{B}^{11}$.¹⁴ However, the complexity of these spectra precludes an analysis of direct population yield to specific levels.

II. EXPERIMENTAL PROCEDURE

The lithium-ion beams are produced in the University of Iowa 5.5-MeV CN Van de Graaff generator. The lithium-ion source is based on the original¹⁵ hot filament ion source of Norbeck. The beam is momentum analyzed by a 90-deg magnet. Energy stabilization is achieved by control slits at the exit of this magnet. The geometry limits the beam energy spread to 11 keV, but the energy stability over long periods is about 5 keV. The energy calibration is established with the $\text{Li}^7(p, n)\text{Be}^7$ threshold reaction to about 5 keV. The beam is deflected 15 deg by a switching magnet into the target-chamber port. Target chamber-entrance apertures are approximately 17 ft from the last quadrupole focusing lens.

A. Scattering Chamber

The 8-in. scattering chamber has been described previously.¹⁶ The chamber is tilted 20.5 deg with respect to the beam direction; the movable dE/dx , E detector is inclined 20.5 deg with respect to the chamber

¹⁰ N. Austern, R. M. Drisko, E. C. Halbert, and G. R. Satchler, Phys. Rev. **133**, B3 (1964).

¹¹ J. M. Blatt and V. F. Weisskopf, *Theoretical Nuclear Physics* (John Wiley & Sons, Inc., New York, 1962), p. 361; W. T. Sharp, H. E. Gove, and E. B. Paul, Chalk River Project, 1955 (unpublished).

¹² N. MacDonald, Nucl. Phys. **33**, 110 (1962).

¹³ T. Ericson, Phys. Rev. Letters **5**, 430 (1960).

¹⁴ E. Norbeck, S. A. Coon, R. R. Carlson, and E. Berkowitz, Phys. Rev. **130**, 1971 (1963).

¹⁵ E. Norbeck, Phys. Rev. **105**, 204 (1957).

¹⁶ R. R. Carlson, R. L. McGrath, and E. Norbeck, Phys. Rev. **136**, B1687 (1964); R. L. McGrath, University of Iowa Report 65-27, 1965 (unpublished).

so that measurements in the angular range of 0 to 139 deg are possible. A single monitor detector mounted at 90 deg relative to the beam direction is used to normalize data. The defining aperture of the E detector is 0.169 ± 0.004 in. in diameter and is 3.735 ± 0.010 in. from the chamber center; the solid angle is $(1.617 \pm 0.077) \times 10^{-3}$ sr. The beam spot is about 0.080 in. in diameter. A foil wheel in front of the proportional counter permits various Al foils to be inserted in front of the entrance window to keep scattered beams from entering the counter.

A Faraday cup can be rotated to 0 deg with respect to the incident beam when the dE/dx , E detector is at 42.1 deg (laboratory). This cup is equipped with a ring magnet, and grid at -300 V in order to suppress secondary electrons.

The target chamber has been checked for asymmetries, and systematic errors by elastically scattering protons on Au¹⁹⁷ and C¹² foils at 4.65 MeV; the C¹² results have been compared with measurements at two other laboratories.¹⁷ Finally, angular distributions of the first three proton groups from the C¹²(He³, p)N¹⁴ reaction have been compared with previous work¹⁸ at 2.666 MeV. In general, agreement with comparison work is found within errors.

B. Targets

Targets are mounted on frames with 0.375-in. holes and placed at ± 120 deg (laboratory) with respect to the incident beam. The Li⁶+B¹¹ reactions were studied using a 1.7 mg/cm² Al backed target. Very large amounts of C¹² and O¹⁶ contamination were observed; in addition, after several hours of bombardment (current about 0.2 μ A) lithium contamination was also present. Consequently, self-supporting boron films have been used to study the remaining three sets of reactions.

The targets are prepared by evaporation of amorphous boron loaded in Ta boats. The boron is heated by electron bombardment, and deposited on glass slides previously coated with "Teepol" solution. The boron is later floated off the slides and mounted on target holders. The B¹¹ enrichment is 98.5%, B¹⁰ is 92.5% enriched with about 7.5% B¹¹ contaminant.

Target thicknesses are measured by observing the apparent energy shift in the Li⁷(p,n)Be⁷ threshold reaction in passing a mass-2 proton beam through the boron foil. Using experimental values of proton energy loss per μ g/cm² in carbon¹⁹ combined with theoretical estimates of the energy loss ratio for boron compared to

carbon²⁰ it is found that the B¹⁰ target is 17.9 ± 3.1 μ g/cm² and the B¹¹ target is 68.0 ± 3.4 μ g/cm² thick. The targets are effectively 1.5 times thicker than this since the targets are not normal to the beam direction. The measured²¹ stopping power of N₂ gas for lithium ions may be converted to B¹⁰, B¹¹ to obtain the energy loss in the target for each reaction: 74 keV (Li⁶+B¹⁰); 83 keV (Li⁷+B¹⁰), 280 keV (Li⁶+B¹¹), 320 keV (Li⁷+B¹¹). It should be noted that this B¹¹ target is not used for angular distribution measurements, but only for absolute-cross-section measurement. The B¹¹ targets used to measure angular distributions are estimated to cause about 85-keV (Li⁶+B¹¹) and 160-keV (Li⁷+B¹¹) energy loss.

C. Data Acquisition

The dE/dx , E detector consists of a proportional counter with a solid-state lithium-drifted silicon detector mounted inside. A 0.0001-in. Mylar film covers the entrance aperture; this is equivalent to about 0.6 mg/cm² of Al. A 95% Ar, 5% CO₂ mixture at about 0.5 atm pressure is used in the proportional counter (the stopping power is equivalent to 4.7 mg/cm² Al). The anode voltage is 1500 V; the anode resistor is chosen to make the pulse decay time about 100 μ sec.

The E detector has a sensitive area of 1 cm². The depletion depth is 2000 μ at 150 V bias; this is approximately the range of 20-MeV protons. The gold surface "dead layer" is measured with Th B alphas to be 0.2 ± 0.1 mg/cm² Al equivalent. The monitor counter is an n - p junction detector with a 200- μ depletion depth. It is covered with an 8 mg/cm² Al foil.

Figure 1 shows the electronics arrangement, which has been described previously.¹⁶ The monitor pulses are amplified, fed into a single-channel window and to a scaler.

The multiparameter pulse-height analysis system described by Carlson and Norbeck²² analyzes the dE/dx , E pulses. Nuclear Data 160 F analog to digital converters perform 1024-channel pulse-height analysis on both pulses. The E pulse is also fed into a discriminator which provides gate pulses to trigger the analog to digital converter units and the Control Data 160-A computer. Both 10-bit words, containing the pulse-height information, are read into the computer and subsequently written on magnetic tape. The words are also condensed and stored in the computer memory. The average analog to digital conversion and computer analysis times are each about 150 μ sec per event. In operation never more than 60 events per second are analyzed: The dead time correction is thus always less than 1%.

¹⁷ H. von Schneider, *Helv. Phys. Acta* **29**, 55 (1956); C. W. Reich, G. C. Phillips, and J. L. Russell, *Phys. Rev.* **104**, 143 (1956).

¹⁸ D. A. Bromley, E. Almqvist, H. E. Gove, A. E. Litherland, E. B. Paul, and A. J. Ferguson, *Phys. Rev.* **105**, 957 (1957).

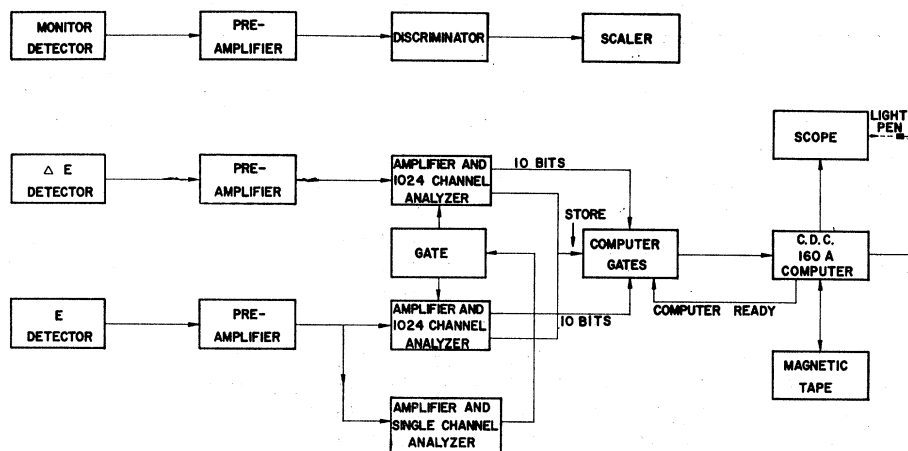
¹⁹ W. Whaling, in *Handbuch der Physik*, edited by S. Flügge (Springer-Verlag, Berlin, 1958), Vol. 34, p. 193.

²⁰ L. C. Northcliffe, in *Annual Review of Nuclear Science*, edited by E. Segrè (Annual Reviews, Inc., Palo Alto, California, 1963), Vol. 13, p. 67.

²¹ S. K. Allison, D. Anton, and R. A. Morrison, *Phys. Rev.* **138**, A688 (1965).

²² R. R. Carlson and E. Norbeck, *Phys. Rev.* **131**, 1204 (1963).

FIG. 1. Block diagram of electronics.



A $60 (dE/dx) \times 128(E)$ array of the counters of the computer memory is displayed on an oscilloscope while the experiment is in progress. A typical display is shown in the upper part of Fig. 2. The ionization energy loss rate of charge-two particles is much larger than that of charge-one particles; hence helium dE/dx pulses lying between channels 240 and 1024 are not shown, to allow the charge-one particles to be observed in greater detail in this display.

After completion of the experiment, the data stored on the tape are read back into the computer and various operations are programmed into the computer so that energy spectra of the desired charged particle may be extracted. The 8192-word memory core restricts possible methods for efficiently analyzing the 1024×1024 array of data. A simple, fast method is to condense large blocks of this array to 60×128 so that most of the array is displayed after one scan of the original data. Subsequent marking of this array with a light pen connected to the computer results in the ionization curve of one kind of particle being "projected" onto the energy axis. Unfortunately, the inherently poor resolution of pro-

portional counters compounded by the small energy loss of charge-one particles in the counter precludes this method (our counter is measured to have 30% resolution for a 10-MeV proton in 0.5-atm gas). The alternative method of scanning 60×128 blocks of the entire 1024×1024 array (4×128 words are reserved for computer programs) is prohibitively time consuming since the ionization curves would require an average of 20 scans of a single run in order to mark interesting areas.

This problem is alleviated by scanning the original data written in E , dE/dx format, taking the product $(E+E_0) \times (dE/dx)$, where E_0 is an arbitrary constant, and writing the new format E , $((E+E_0) + (dE/dx))$ on tape; the point being that for particle energies well described by the Bethe-Bloch energy loss formula the product $(E) \times (dE/dx)$ is proportional to MZ^2 , where M and Z are the mass and charge of the particle. Thus the curved ionization curves are transformed to approximately parallel straight lines. Analog pulse multipliers are widely used in this application; however digital multiplication introduces no loss of resolution.

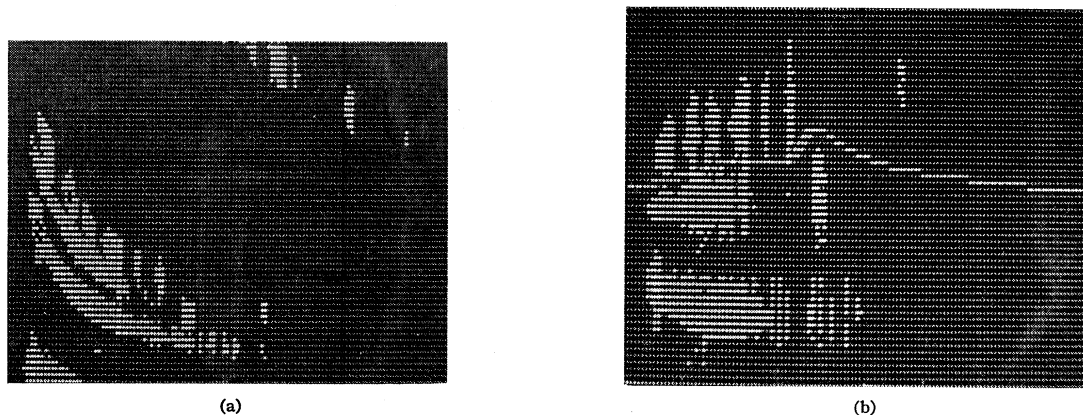


FIG. 2. (a) This photograph shows condensed $60 \times 128 dE/dx$, E contour display of p , d , t , and α particles from the $\text{Li}^7 + \text{B}^{11}$ reactions. (b) This photograph shows the same data after multiplication. The y axis $[dE/dx(E+E_0)]$ is shown full scale but the 1024-channel x axis (E) is condensed to 128 channels. A light pen mark is visible between the d and t groups.

A section of the transformed data is scanned with full detail (6 bits) in the $(E+E_0) \times (dE/dx)$ direction, set so as to encompass charge-one particles, and 128 channels (condensed by a factor of 8) in the E direction. This array is shown in the lower part of Fig. 2. Thus one scan (with no loss of resolution) suffices to obtain all data except those on helium when both He^3 and He^4 are produced. In most of the reactions, He^3 particles are produced with much less energy than alpha particles. In these cases large values of dE/dx usually indicate an alpha particle rather than He^3 so the value of dE/dx is not recorded in the original data but in its place a constant is stored. This constant is used to flag the alphas and is used in place of the above product to denote mass. A line showing a light pen mark appears in the figure. After appropriate marking with the light pen, the tape is scanned once more. All events in a given E channel and between the marks defining a particle group are summed to produce an energy spectrum of this group. The particle types are essentially completely resolved with this method. The 1024-channel spectra are displayed by the computer. Finally the positions and number of counts in peaks in the spectra are read out of the computer.

D. Data Analysis

In most cases measurements are made at 5-deg intervals from 10 to 80 deg (laboratory) and 10-deg intervals from 80 to 140 deg (the $\text{Li}^6 + \text{B}^{11}$ data are taken every 10 deg). The monitor scaler reading is used to normalize data taken at various angles. Absolute cross sections are determined by integrating the beam passing through the targets when the movable detector is at 42.1°. The charge equilibrium value for lithium ions at 5 MeV is taken to be 2.83 ± 0.10 .²³

At each angle the peak channel numbers are plotted versus energies previously calculated with a FORTRAN kinematics program (PEP). The program computes particle energies after passing through all absorbing materials for all known residual energy levels. Energies of carbon, oxygen, and lithium-lithium contaminant products are also calculated. Except for carbon buildup under bombardment and some oxygen from B_2O_3 , contamination problems are eliminated with thin self-supporting targets. Parts of some angular distributions, are not given where contaminant groups coincide with the peak of interest. The reaction products from the 8% B^{11} component in the B^{10} targets are ignored except for several large yield B^{11} reactions discussed below.

Calibrations of energy spectra are determined by estimating which peaks correspond to known levels and plotting channel number versus calculated energy until self-consistent results are found for all angles. In general these calibrations are accurate to 50 keV; a few cases which are mentioned below have 30-keV accuracy.

The number of counts in peaks at each angle, total

²³ C. S. Zaidins, California Institute of Technology, 1962 (unpublished).

charge deposited on the target during the absolute-cross-section measurement at 42.1 deg, and other parameters are fed into another FORTRAN program which calculates differential and integral cross sections. The trapezoidal rule is used in the integration. The integrated results are multiplied by a factor to give the "total" cross section from 0 to 150 deg. This factor is computed on the assumption that $d\sigma/d\Omega$ over the unobserved angular range is equal to the average $d\sigma/d\Omega$ over the observed angles. Most measurements cover the angles 0 to approximately 145 deg in the center-of-mass system. In a few cases, however, cross sections are presented for groups observed over much smaller ranges. These numbers must obviously be regarded with caution.

E. Errors

The differential-cross-section errors for resolved particle groups shown in Figs. 30 through 38 are about 1.25 times the statistical standard deviation error. This factor is based on reproducibility checks before and after each set of angular distributions; it results from carbon buildup on targets, electronic drifts, and random errors caused by slight overlap between different particle types. The random errors cause an error in the relative total-cross-section measurements on the order of $[1/\sqrt{(2N)}](\Delta y/y)$, where N is the number of angles and $(\Delta y/y)$ is the error associated with a typical datum point of the differential cross sections. For example, the relative cross-section random error for the $\text{B}^{10}(\text{Li}^6, d)\text{N}^{14}$ g.s. reaction is about 2%. It is estimated that systematic errors (caused for the most part by the experimenter's computer light pen marking habits) are on the order of 5%. The size of this error is determined in part by the degree to which the particle type is resolved from other kinds of particles. The extrapolation over unobserved angles contributes an unknown error. Uncertainties in target thickness, solid angle, current integration, and lithium effective equilibrium charge are estimated to be, respectively: 17% (B^{10}), 5% (B^{11}); 5%, 2%, and 10%. Thus, absolute cross sections have errors of about 22% (B^{10}) and 15% (B^{11}).

III. ENERGY SPECTRA

Spectra at 20 deg are shown in Figs. 3 through 19. The abscissas are labeled by channel number and observed particle energy. The E detector depletion depth is sufficient to stop 20-MeV protons. Charge-one particles have typical peak widths for narrow residual levels of about 110 keV; broadening is evident in alpha spectra because of absorbing materials in front of the E counter (ranging from 11.4 to 5.5 mg/cm² Al equivalent).

Peaks are assigned to energy levels given in the 1962 compilation by Lauritsen and Ajzenberg-Selove²⁴ unless

²⁴ T. Lauritsen and F. Ajzenberg-Selove, in *Nuclear Data Sheets*, compiled by K. Way, *et al.* (Printing and Publishing Office, National Academy of Sciences-National Research Council, Washington 25, D. C., 1962), NRC 61-5-6.

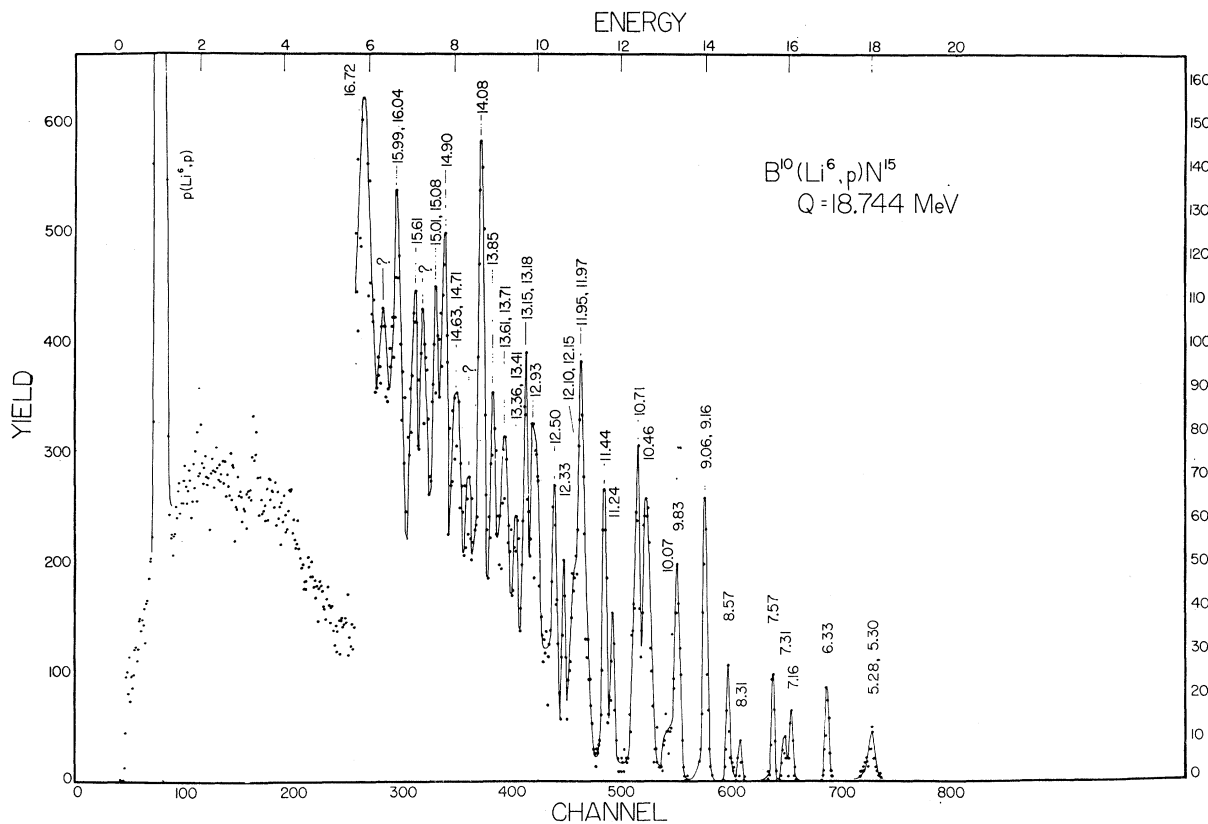


FIG. 3. $\text{B}^{10}(\text{Li}^6, p)\text{N}^{15}$ spectrum at 20 deg. The abscissa is marked by channel number and by particle energy. The ordinate gives the number of counts. Most of the numbers labeling peaks are taken from energy level data in Ref. 24. Exceptions are discussed in the text. The energy calibration is accurate to ± 0.05 MeV.

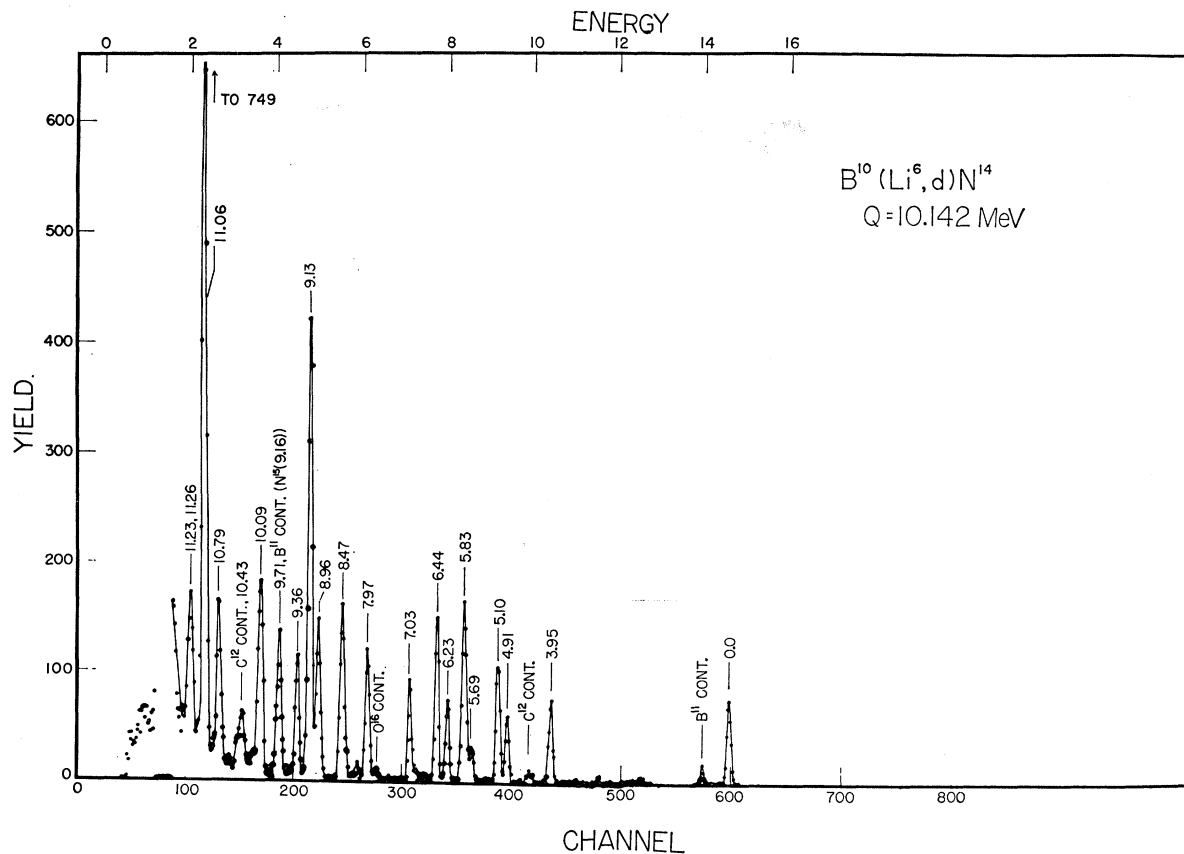


FIG. 4. $\text{B}^{10}(\text{Li}^6, d)\text{N}^{14}$ spectrum. See caption Fig. 3. The energy calibration below 7 MeV is accurate to ± 0.03 MeV.

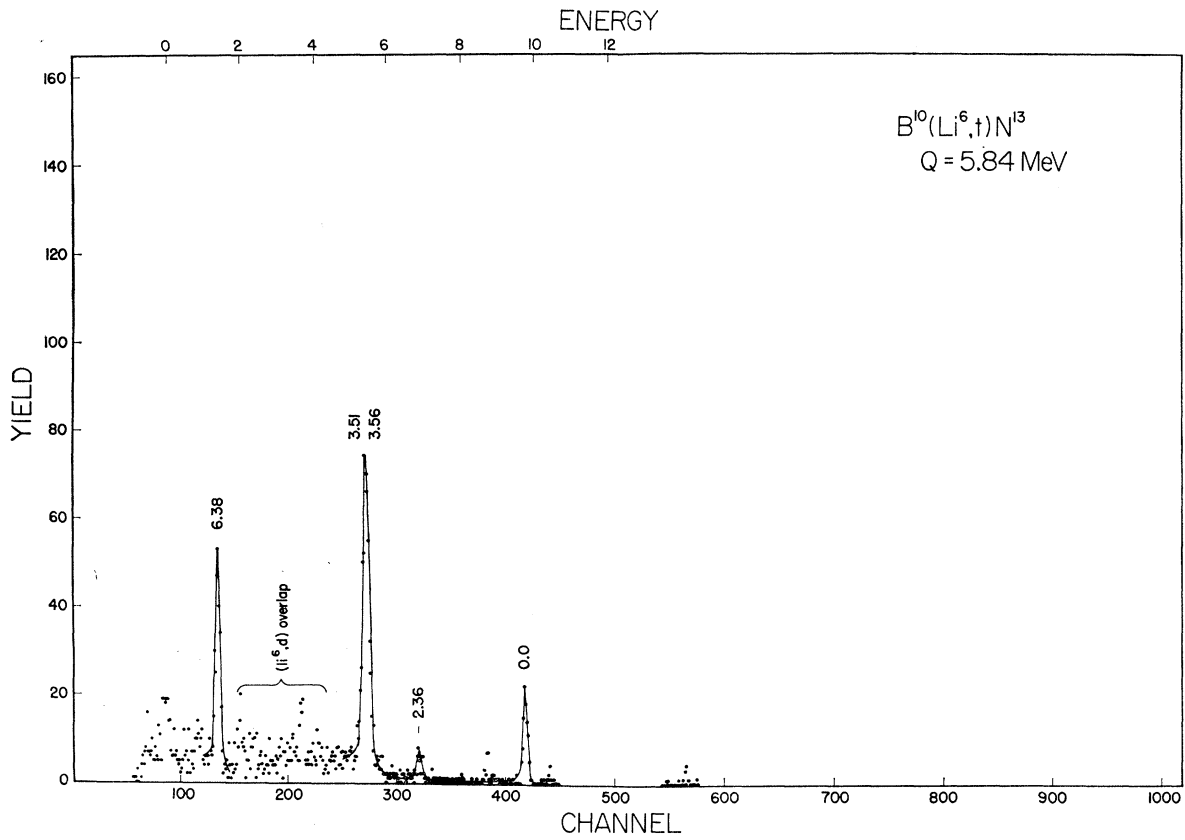


FIG. 5. $B^{10}(Li^6,t)N^{13}$ spectrum. See caption Fig. 3. Part of the background is due to deuteron overlap.

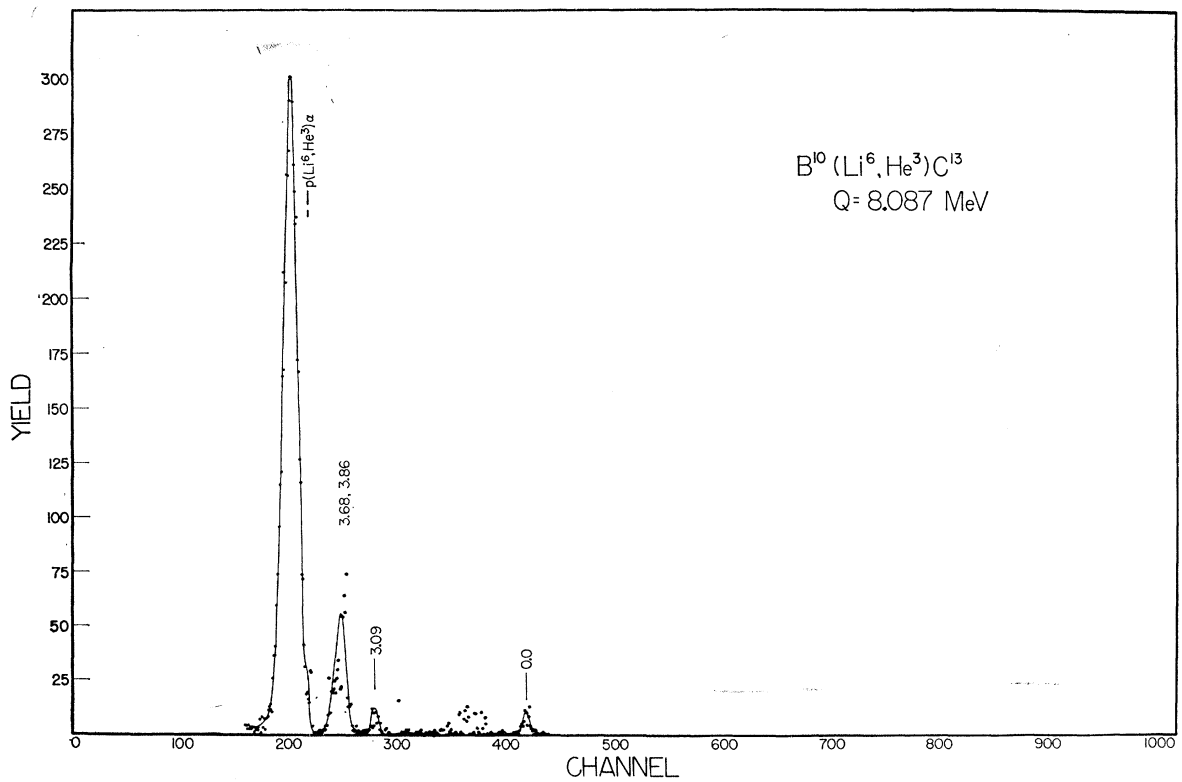


FIG. 6. $B^{10}(Li^6,He^3)C^{13}$ spectrum. See caption Fig. 3. The large peak near cutoff is from target hydrogen contamination.

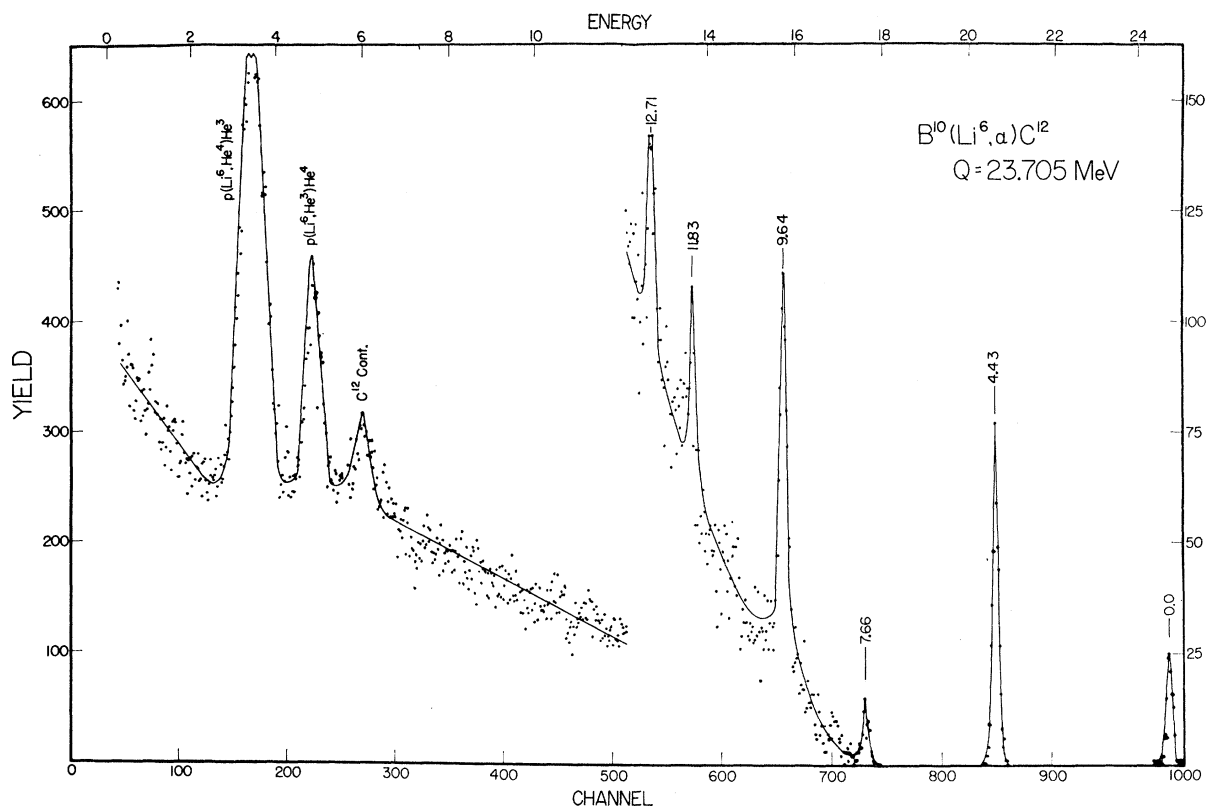


FIG. 7. $\text{B}^{10}(\text{Li}^6, \alpha)\text{C}^{12}$ spectrum. See caption Fig. 3. The low-energy peaks are due to hydrogen and C^{12} contamination.

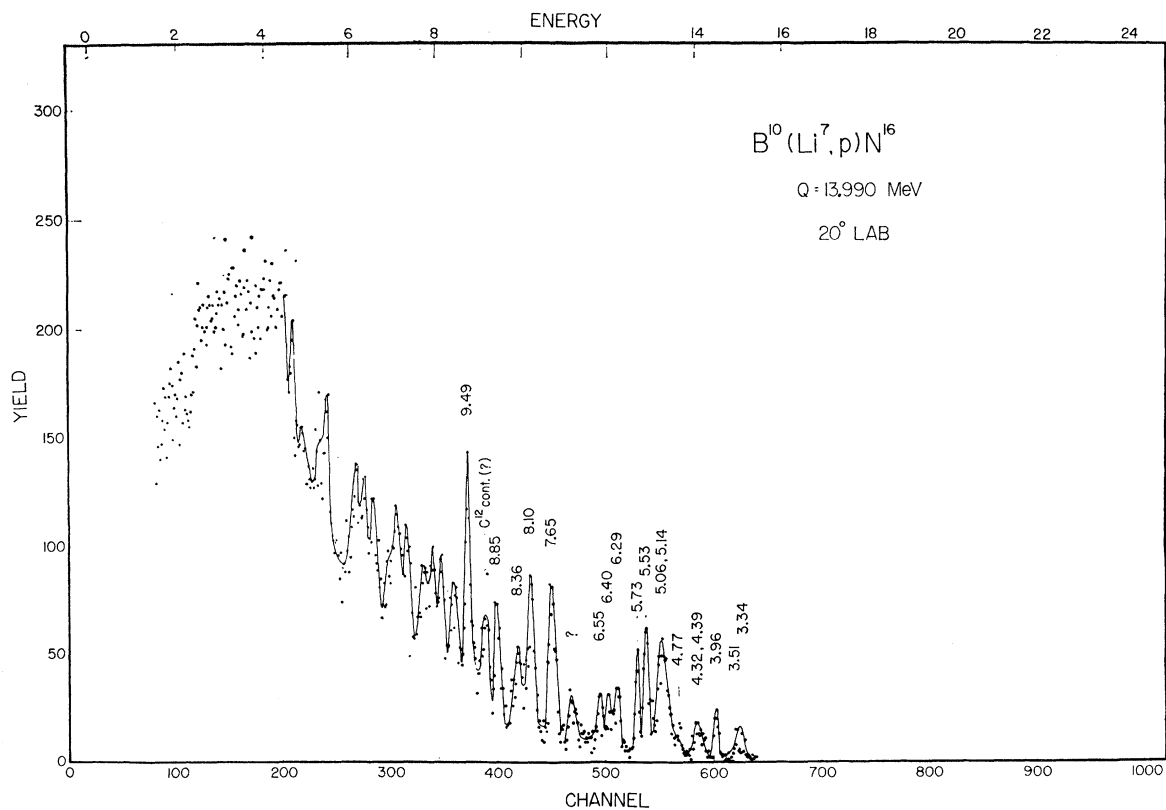


FIG. 8. $\text{B}^{10}(\text{Li}^7, p)\text{N}^{16}$ spectrum. See caption Fig. 3. Because of C^{12} contamination, peaks with less than about 8.5-MeV energy are not assigned.

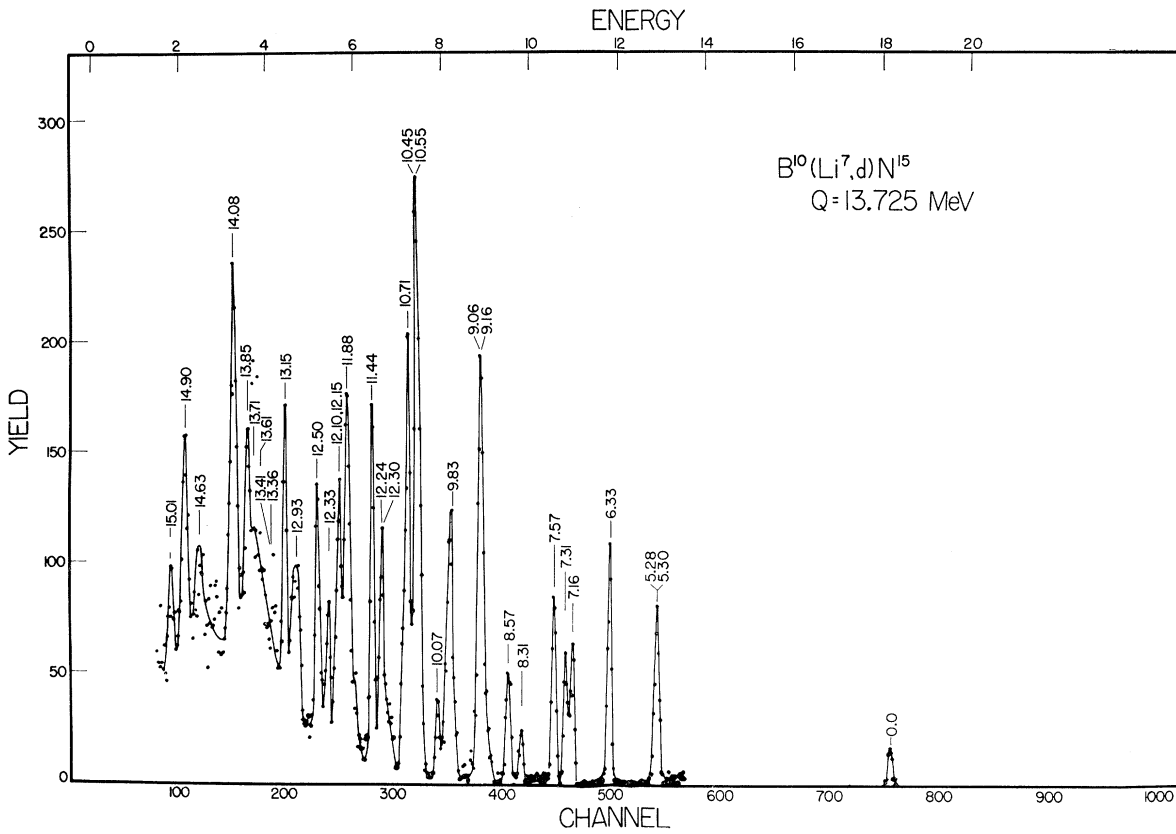


FIG. 9. $B^{10}(Li^7,d)N^{15}$ spectrum. See caption Fig. 3.

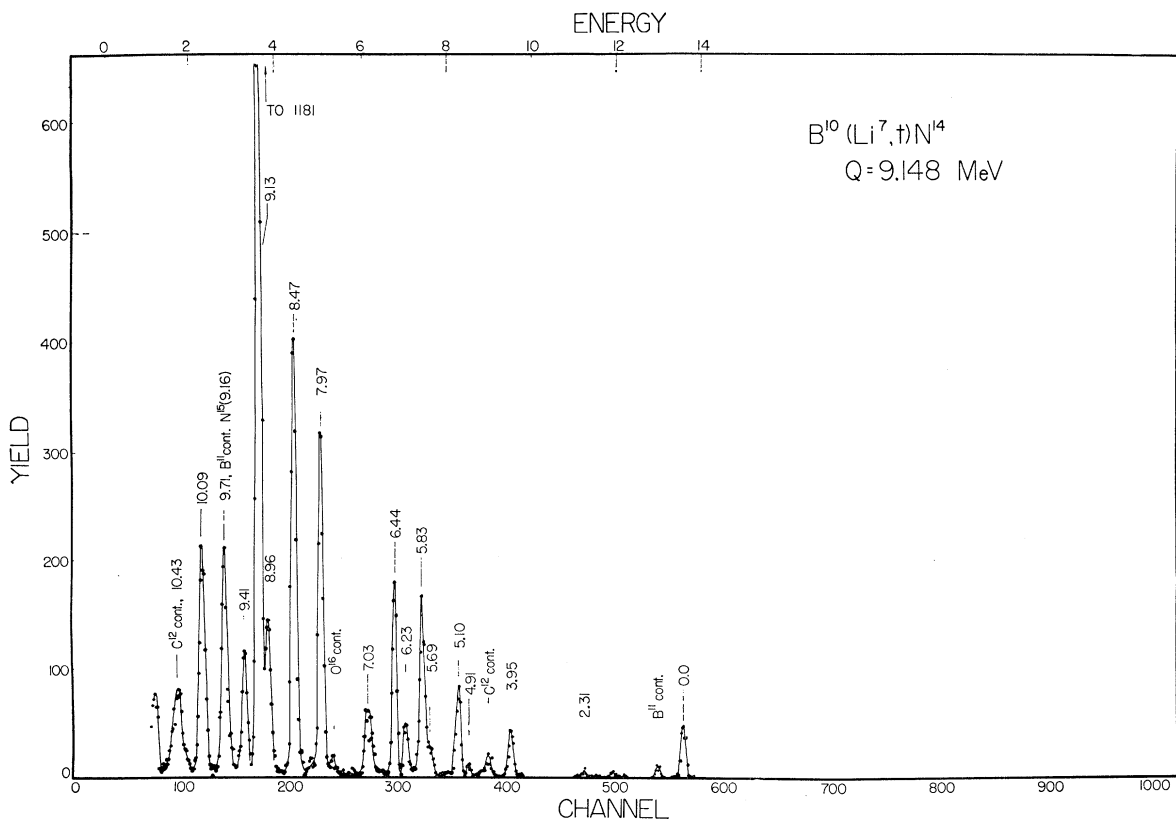


FIG. 10. $B^{10}(Li^7,t)N^{14}$ spectrum. See caption Fig. 3. The energy calibration below 6 MeV is accurate to ± 0.03 MeV.

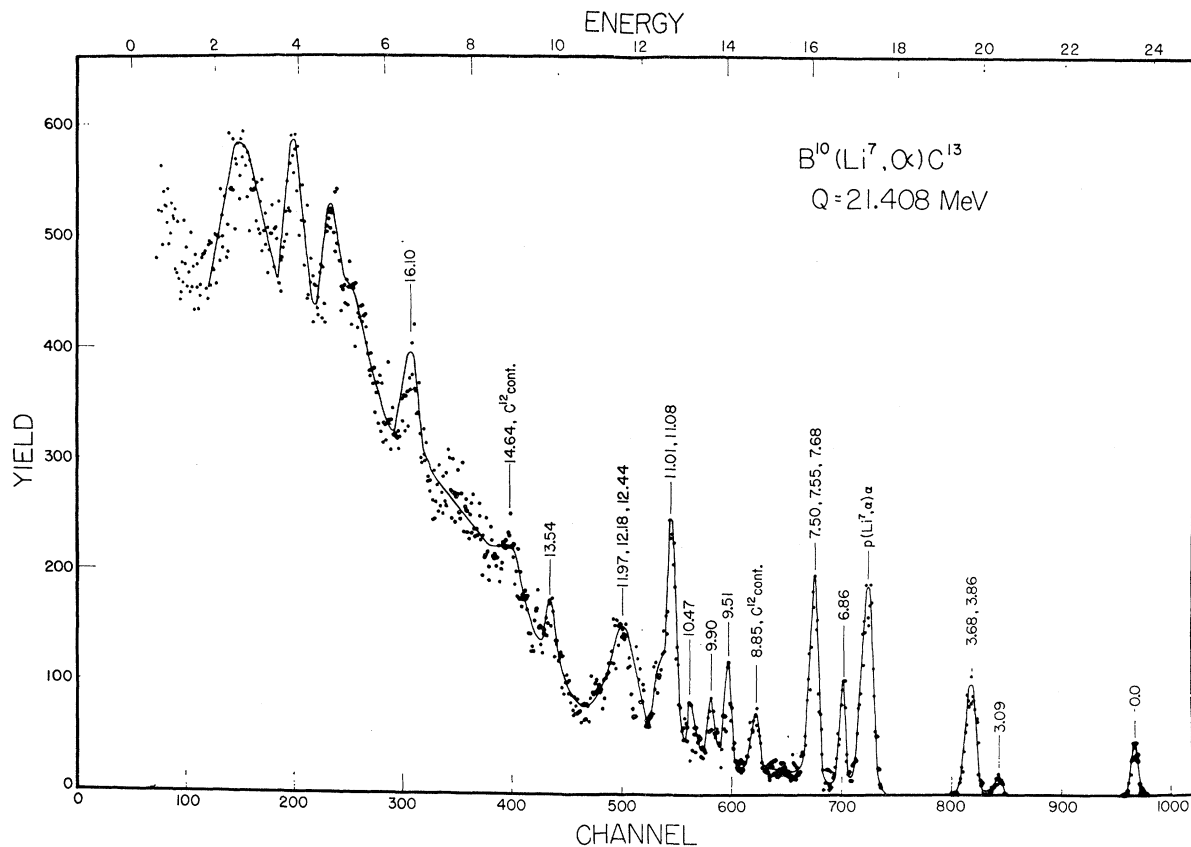


FIG. 11. $\text{B}^{10}(\text{Li}^7, \alpha)\text{C}^{13}$ spectrum. See caption Fig. 3. The three low-energy peaks are due to C^{12} contamination, $\text{B}^{10}(\text{Li}^7, \text{He}^3)\text{C}^{13}$, and/or unreported C^{13} levels.

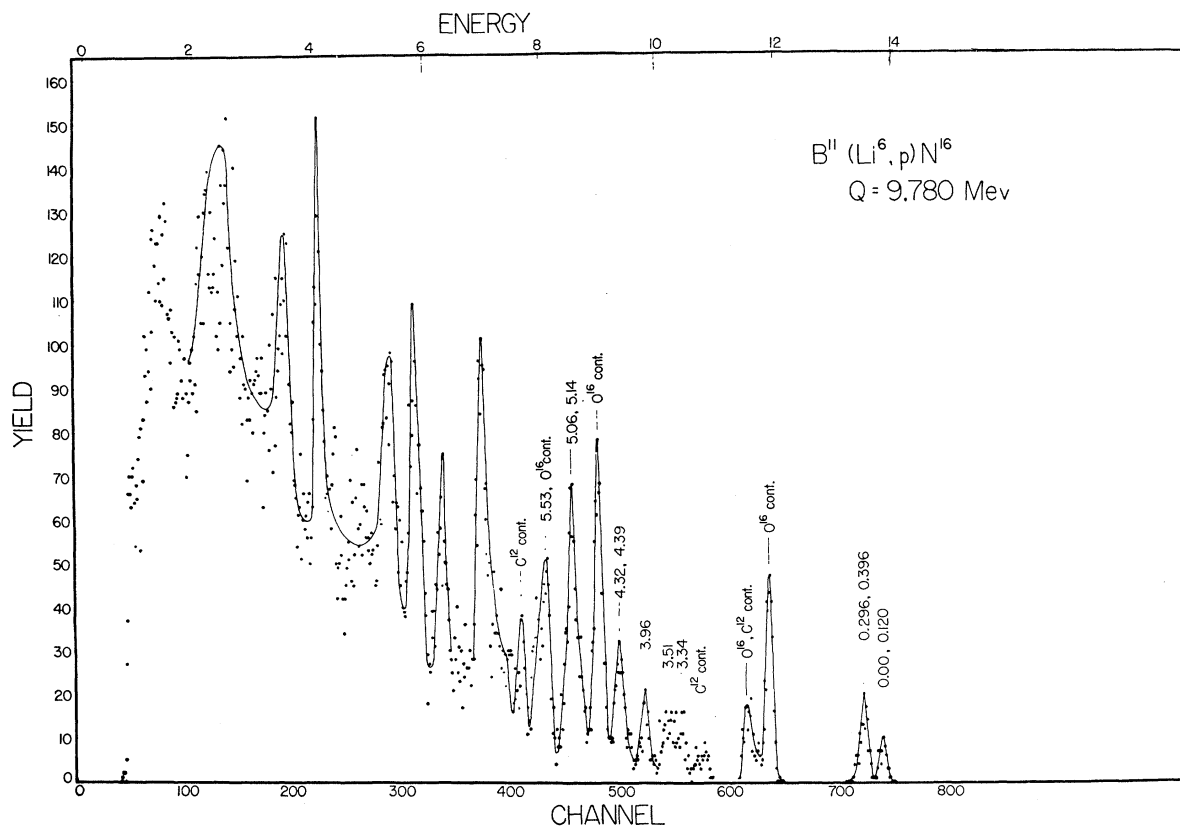


FIG. 12. $\text{B}^{11}(\text{Li}^6, p)\text{N}^{16}$ spectrum. See caption Fig. 3. C^{12} , O^{16} contaminants preclude unambiguous assignments to peaks with less than 7-MeV energy.

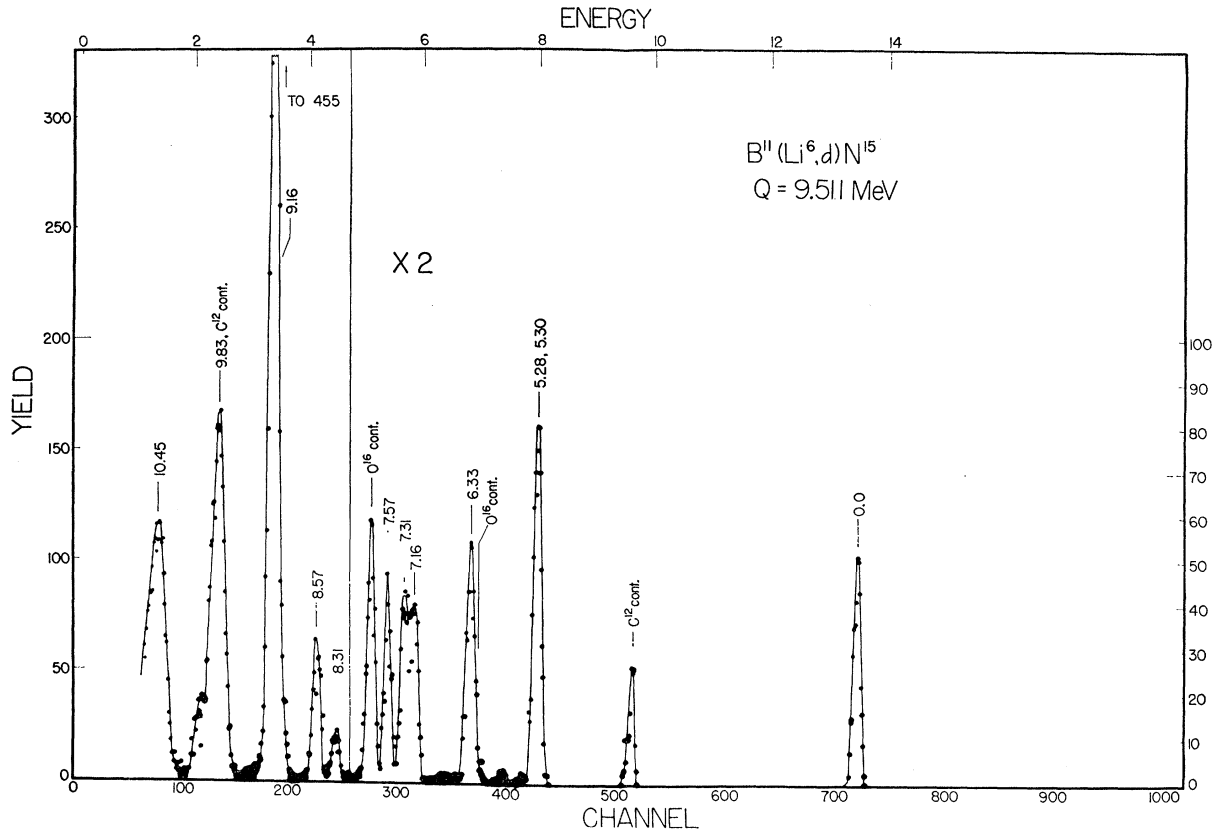


FIG. 13. $B^{11}(Li^6,d)N^{15}$ spectrum. See caption Fig. 3.

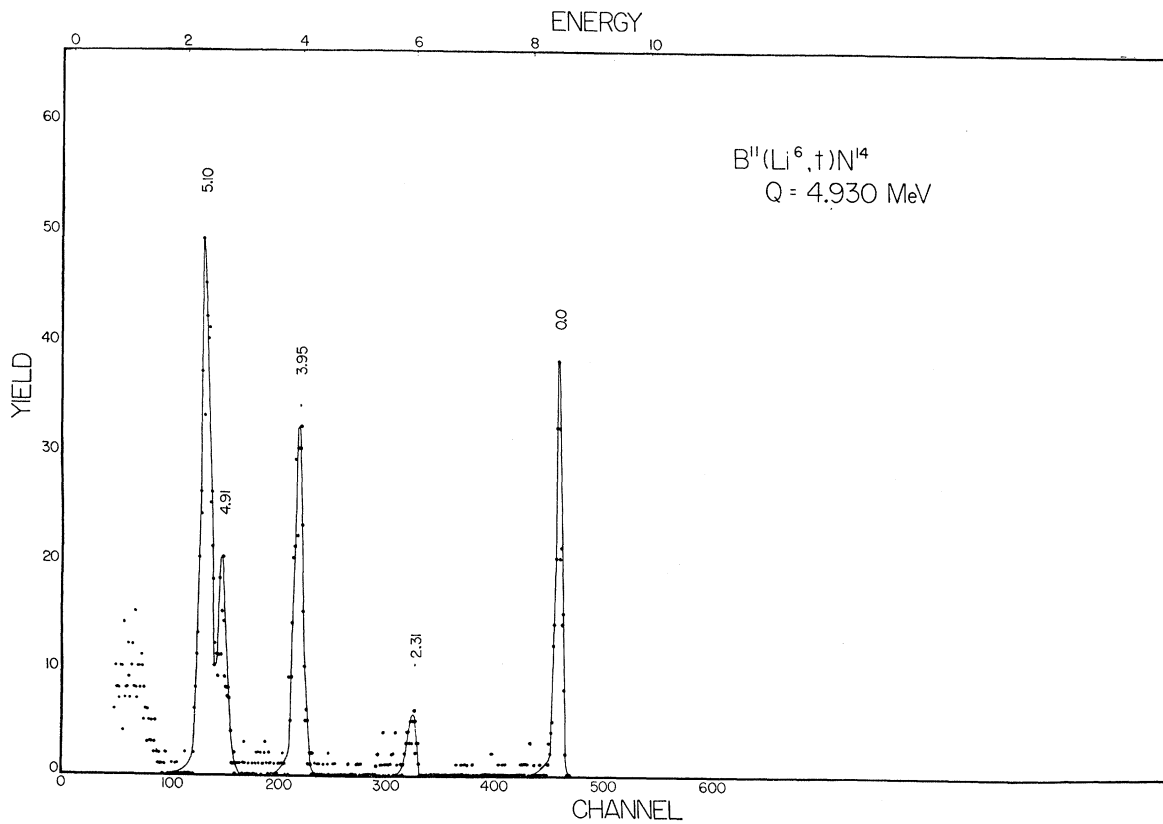


FIG. 14. $B^{11}(Li^6,t)N^{14}$ spectrum. See caption Fig. 3.

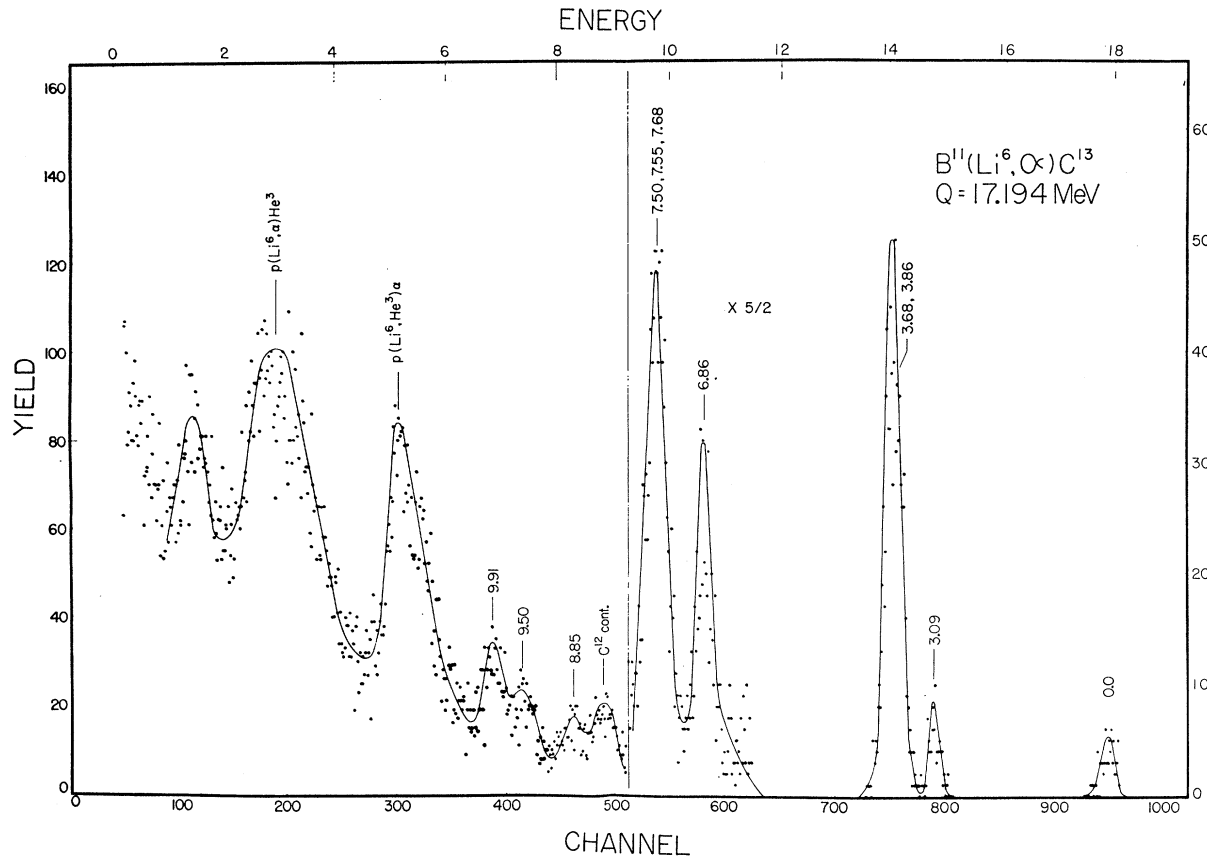


FIG. 15. $\text{B}^{11}(\text{Li}^6, \alpha)\text{C}^{13}$ spectrum. See caption Fig. 3. Peaks having less than 6 MeV are due to contaminants.

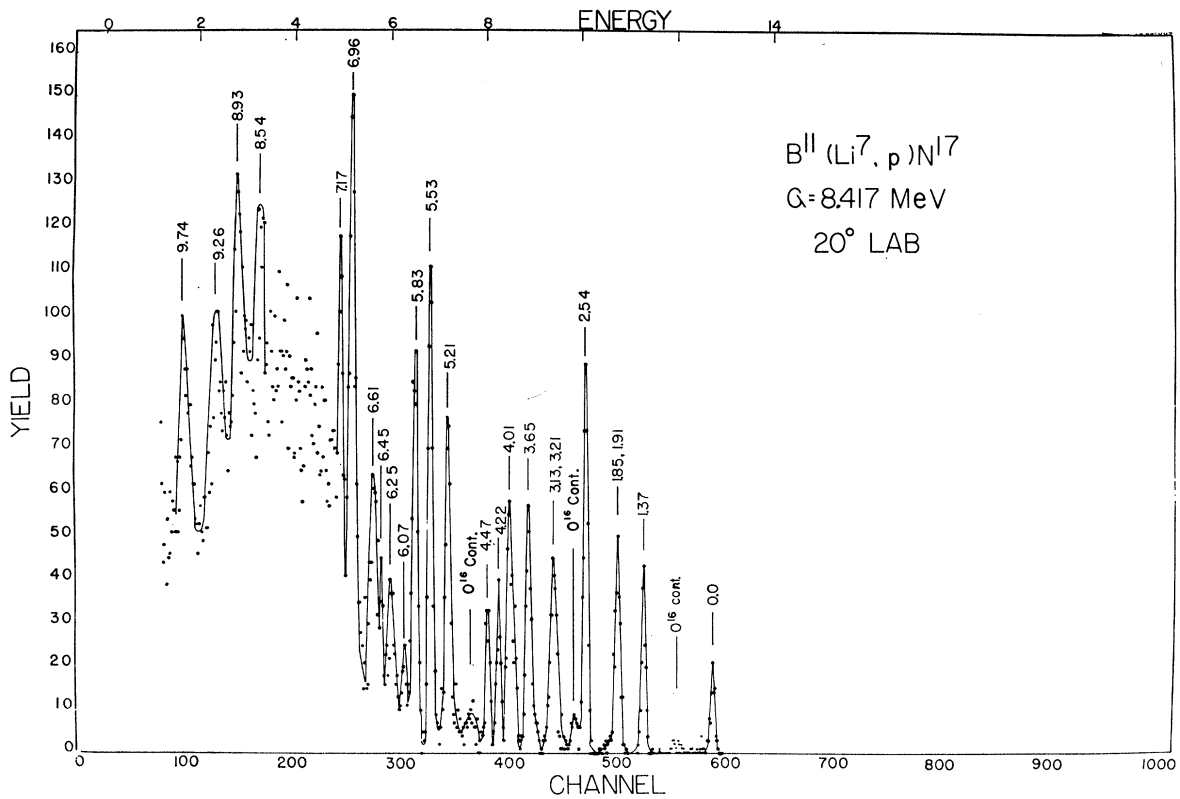
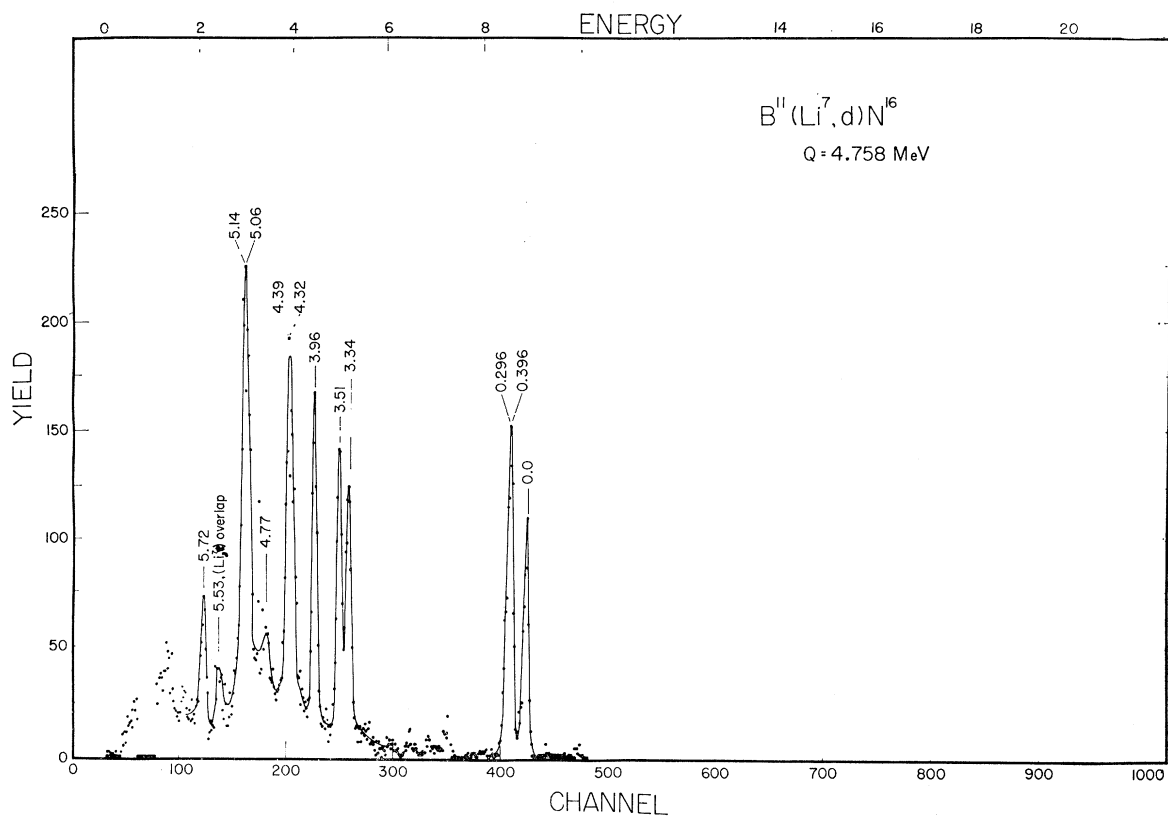
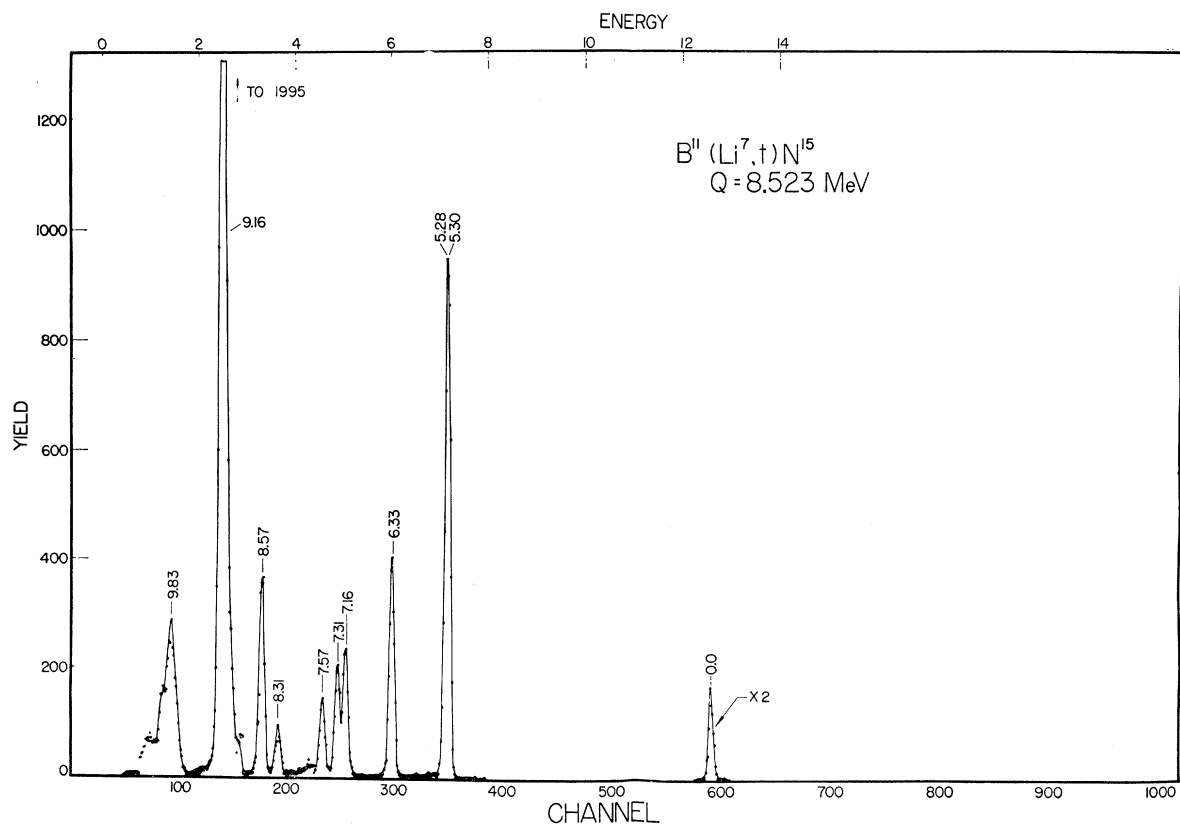


FIG. 16. $\text{B}^{11}(\text{Li}^7, p)\text{N}^{17}$ spectrum. See caption Fig. 3. Peaks corresponding to levels between 7.17 and 8.54 MeV are distinct at back angles.

FIG. 17. $B^{11}(Li^7,d)N^{16}$ spectrum. See caption Fig. 3.FIG. 18. $B^{11}(Li^7,t)N^{15}$ spectrum. See caption Fig. 3.

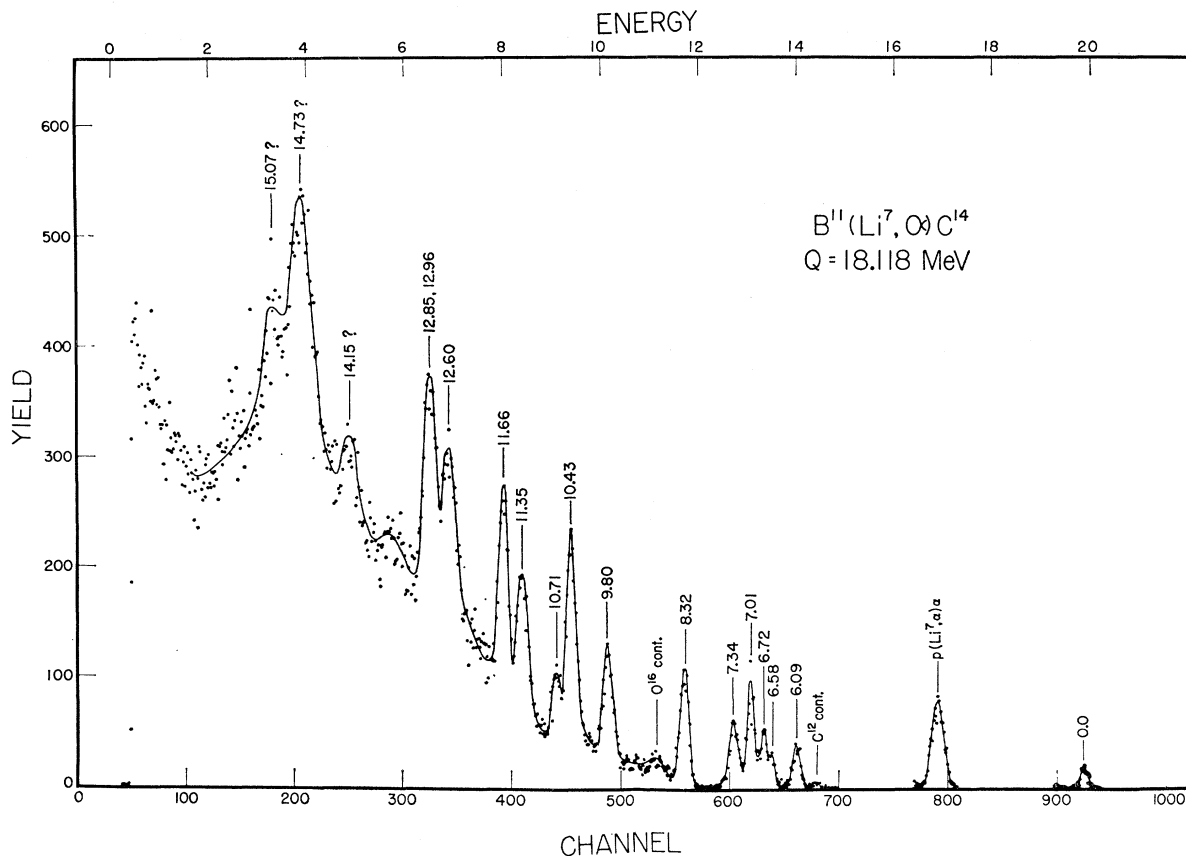


Fig. 19. $\text{B}^{11}(\text{Li}^7, \alpha)\text{C}^{14}$ spectrum. See caption Fig. 3. The peaks labeled by question marks are not observed at enough angles to establish unambiguously that they correspond to unreported C^{14} levels (see text).

referenced otherwise. Several previously unreported levels are found. Often spectra have large continuum backgrounds which obscure reported levels at the higher excitation energies. At lower excitations almost all known levels are populated; the few exceptions are discussed below.

A. $\text{Li}^6 + \text{B}^{10}$

About 30 groups corresponding to N^{15} levels are identified in Fig. 3. The ground-state group is not stopped in the E counter. The large continuum can be caused by any of several competing reactions. For example: $\text{N}^{14} + p + n + 7.0$ MeV; $\text{C}^{14} + 2p + 8.6$ MeV; $\text{C}^{13} + d + p + 2.4$ MeV; $\text{C}^{13} + 2p + n - 0.3$ MeV; $\text{C}^{12} + t + p + 3.9$ MeV; and $\text{B}^{11} + \alpha + p + 7.6$ MeV. The peak near the low-energy cutoff is caused by elastically scattered protons contaminating the target.

Twenty peaks corresponding to known levels of N^{14} are observed in Fig. 4. Isotopic spin selection rules forbid the population of $T=1$ states. In fact, the 2.31-MeV $0+$ state has a cross section about 0.072 that of the 4.91-MeV $0(-)$ state. Isotopic spin violations to this level have been observed²⁵ before and attributed to

²⁵ J. Cerny, R. H. Pehl, E. Rivet, and B. G. Harvey, Phys. Letters 7, 67 (1963); D. H. Wilkinson, Phil. Mag. 1, 379 (1956).

isospin mixing in the compound nucleus. The $T=1$ states at 8.06, 8.63, 8.71, and 9.51 MeV are not observed. All known $T=0$ levels are populated except those at 6.05, 6.70, 7.40, and 7.60 MeV. These levels have not been observed in other²⁶ experiments, hence it may be surmised that either they are $T=1$ states or do not exist. The peak corresponding to the 9.71-MeV state is dominated by deuterons from the large yield $\text{B}^{11}(\text{Li}^6, d)\text{N}^{15}$ (9.16 MeV) contaminant reaction.

Several peaks corresponding to states at high excitations have very large relative yields. The 11.06- and 9.13-MeV levels have cross sections about 2 and 1.5 times larger than any other level. Giant cross sections have been observed^{26,27} in the two-nucleon transfer (α, d), (He, p) reactions leading to a $5+$ level at 9 ± 0.2 MeV. The only other level in this energy region was thought to be the 9.17-MeV $T=1$ level. In order to investigate this region of excitation carefully, the small Q reactions $\text{Li}^6(\text{Li}^7, d)\text{B}^{11}$ and $\text{Li}^6(\text{Li}^6, d)\text{B}^{10}$ are used for energy calibration purposes. The energies of deuterons from the low, well-known levels of B^{10} and B^{11} provide

²⁶ R. H. Pehl, E. Rivet, J. Cerny, and B. G. Harvey, Phys. Rev. 137, B114 (1965).

²⁷ B. G. Harvey, J. Cerny, R. H. Pehl, and E. Rivet, Nucl. Phys. 39, 160 (1962).

calibration points over the necessary deuteron energy range. This method of calibration ensures that uncertainties in absorbing material thicknesses are not important so that N^{14} excitation energies are established to ± 30 keV. The large peak observed here corresponds to 9.13 ± 0.03 MeV. A recent²⁸ experiment on "midget" $C^{13}(p,\gamma)N^{14}$ resonances reports new $T=0$ levels at 8.963 and 9.127 MeV having probable spins and parities 5+ and 2-. Our large peak may correspond to the latter state. The 8.96-MeV state is probably the one seen in the (α,d) experiments so that no connection exists between the large peaks observed in the (α,d) and (Li^6,d) reactions. The peak observed here at 8.96 ± 0.03 MeV excitation may be the superposition of the 8.99- and 8.96-MeV $T=0$ levels. In order to establish further whether there is a correlation between the giant yield states observed in (α,d) , (He^3,p) reactions and those observed in (Li^6,d) reactions, the $N^{14}(Li^6,d)F^{18}$ reaction has been examined using a TiN target for a large yield to the 1.1-MeV F^{18} level as seen in the (α,d) experiments.²⁷ None was observed. Of course, there is no obvious reason why a correlation should exist since the (α,d) states are interpreted²⁷ as having a $(1d_{5/2})^2$ configuration.

Figures 5 and 6 from the mirror reactions $N^{13}+t$ and $C^{13}+He^3$ are similar. Since charge-two particles are not collected in $(dE/dx,E)$ format, separate measurements with lower dE/dx gain have been made on He^3 over the angular range from 0 to 60 deg.

The characteristically large alpha continuum tends to obscure peaks corresponding to states of C^{12} above about 12-MeV excitation in Fig. 7. Large He^3 and alpha peaks from the proton contaminant reaction $p(Li^6,\alpha)He^3$ are present along with a peak probably due to C^{12} contamination. Because of the continuum, the 15.11-MeV $T=1$ level which is reported²⁹ to be weakly populated in this reaction cannot be observed. The 10.1- and 10.84-MeV levels are not discernible above background. The 10.1-MeV level has a somewhat dubious history. It has been suggested³⁰ that this state is a "ghost" of the 7.66-MeV level. If so, then it is expected to have a small yield in this reaction. The absence of the 10.84-MeV state is not understood.

B. Li^7+B^{10}

The N^{16} spectrum is shown in Fig. 8. Spectra at various angles are analyzed to find unreported energy levels. The target has non-negligible carbon contamination after being used previously for the Li^6+B^{10} measurements. Consequently, some large peaks are due to the $C^{12}(Li^7,p)O^{18}$ reaction. It is assumed that those peaks which lead to calculated N^{16} excitation energies equal to ± 0.05 MeV at different angles, and which do not correspond to known O^{18} levels actually do corre-

spond to N^{16} levels. These are listed in Table VIII. The peak density corresponding to level excitations greater than 9.5 MeV is too complex to permit unambiguous assignments.

Recently reported levels³¹ at 5.73, 6.29, 6.40, and 6.55 MeV are confirmed. Additional levels at 7.65, 8.10, 8.36, 8.83, and 9.47 MeV are found. All energies have probable errors of ± 0.05 MeV. Total neutron capture experiments³² on N^{15} show twelve levels between 5.67 and 8.02 MeV. The present observation of a level at 7.65 MeV probably includes two states at 7.654 and 7.684 MeV observed by neutron capture.

About thirty peaks representing N^{15} levels are identified in Fig. 9.

The spectrum in Fig. 10 exhibits seventeen peaks corresponding to N^{14} states. The spectrum is similar to that seen from $B^{10}(Li^6,d)N^{14}$ reaction. This is somewhat surprising because there is no general selection rule to forbid population of $T=1$ states in the present reaction. The 2.31-MeV $0+$, $T=1$ state has a cross section 0.45 times the 4.91-MeV $0(-)$, $T=0$ state. Other $T=1$ states at 8.06, 8.63, 8.71, and 9.51 MeV are not observed. An interpretation of the $T=1$ cross sections in terms of reaction mechanisms will be discussed below.

Again, the 6.05-, 6.70-, 7.40-, and 7.60-MeV levels are not seen. The same technique as described above for the $B^{10}(Li^6,d)N^{14}$ reaction gives the excitations of the levels in the vicinity of 9 MeV to ± 30 keV. The yield of the strong peak labeled 9.13 in Fig. 10 is about 2.2 times larger than that of any other level. This is relatively larger than in the $B^{10}(Li^6,d)N^{14}$ reaction; it is possible that the 9.17-MeV $T=1$ state contributes to the peak. Most of the yield to the peak labeled 9.71 MeV is due to the $B^{11}(Li^7,t)N^{15}$ (9.16 MeV) contaminant reaction.

Fourteen peaks are assigned to known C^{13} states in Fig. 11. Proton contamination in the target produces a large $p(Li^7,\alpha)\alpha$ peak. The three low-energy broad peaks in Fig. 11 are possibly due to carbon contamination and the $B^{10}(Li^7,He^2)C^{14}$ reaction, and/or unreported levels in C^{13} .

C. Li^6+B^{11}

The Li^6+B^{11} reactions are studied with a 1.7 mg/cm² Al-backed target. Oxygen and carbon contaminant peaks are comparable in size to the Li^6+B^{11} peaks. After several hours of bombardment, Li^6 contamination is also large. Figure 12 shows a few peaks which are attributable solely to N^{16} .

The N^{15} spectrum is given in Fig. 13. The cross section to the 9.06-9.16-9.23 MeV N^{15} states, labeled 9.16 in the figure, is about six times larger than that of any other resolved level. The energy calibration and narrowness of this peak imply that the dominant yield is to the 9.16-MeV state.

²⁸ R. W. Detenbeck, J. C. Armstrong, A. S. Figuerra, and J. B. Marion, Nucl. Phys. **72**, 552 (1965).

²⁹ R. R. Carlson and M. J. Throop, Phys. Rev. **136**, B630 (1964).

³⁰ F. C. Barker and P. B. Treacy, Nucl. Phys. **38**, 33 (1962).

³¹ T. R. Donoghue, R. A. Blue, J. E. Jackson, C. R. Soltész, and K. J. Stout, Bull. Am. Phys. Soc. **9**, 628 (1964).

³² D. B. Fossan (private communication).

The peak labeled 9.83 includes three closely spaced known levels in N^{15} . The $\text{C}^{12}(\text{Li}^6, d)\text{O}^{16}$ reaction contributes about 70% of the yield to this peak; in addition this reaction contributes about 60% to the peak labeled 10.45. These percentages are derived from data from the C^{12} reaction⁷ and the yield to the resolved O^{16} ground-state deuteron group. Thus the yield to the 9.16-MeV state is *very* intense compared to all other observed levels.

Five N^{14} groups are identified in Fig. 14. No isotopic spin-selection rule forbids population of the 2.31-MeV $0+$, $T=1$ state; however, the cross section is about $\frac{1}{4}$ that of the 4.91-MeV $0(-)$, $T=0$ state.

Peaks in Fig. 15 corresponding to C^{13} states up to the 7.50-, 7.44-, and 7.68-MeV groups have Q values larger than oxygen and carbon contaminant reactions. The remaining peaks cannot be assigned unambiguously.

D. $\text{Li}^7 + \text{B}^{11}$

Energy levels of N^{17} have been examined recently via the same reaction as in the present experiment by

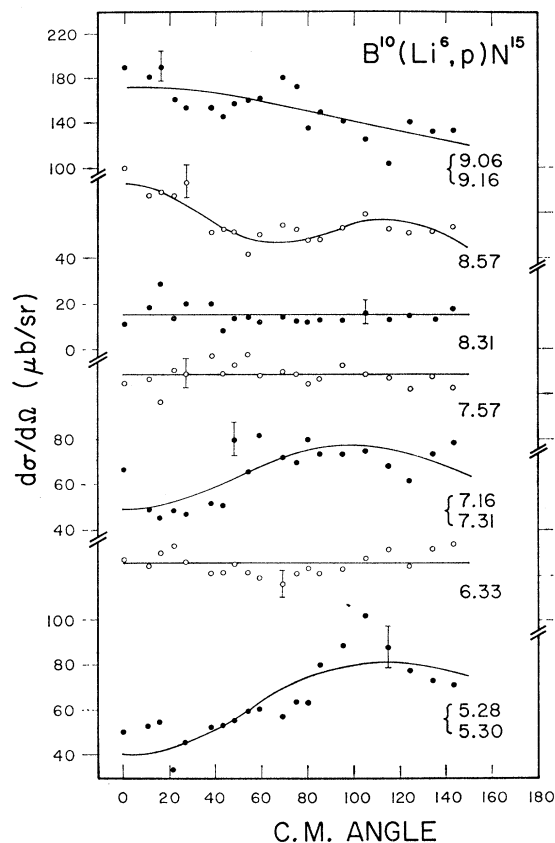


FIG. 20. $\text{B}^{10}(\text{Li}^6, p)\text{N}^{15}$ differential cross sections in $\mu\text{b}/\text{sr}$. Zero levels are suppressed. The ordinate numbers on the left and right correspond to the solid and open data points, respectively. The error bars for resolved levels are given by 1.25 times the statistical errors (see text). The lines through the points represent least mean squares fits to an expansion of Legendre polynomials. The numbers near each curve give the excitation energy of the residual nucleus in MeV.

Hart *et al.*³³ Fourteen new levels were reported between 4.22- and 8.25-MeV excitation energy; three levels were reported as questionable.

The proton energy spectrum is shown in Fig. 16. Excitation energies in N^{17} corresponding to all peaks taken at various angles are tabulated in Table IX. The estimated accuracy is ± 0.04 MeV. All levels previously reported are confirmed. The level at 7.26 MeV is actually a doublet, at 7.17- and 7.37-MeV excitations. Other observed excitation energies agree with those of Hart *et al.* within probable errors except one which was previously reported at 8.25 ± 0.03 MeV; the present

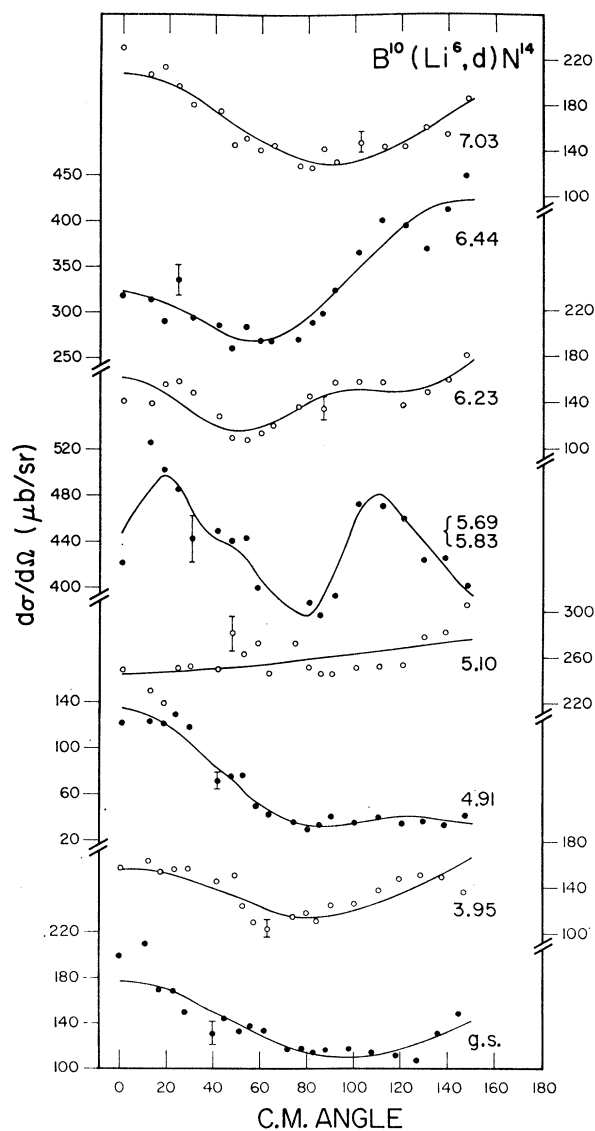


FIG. 21. $\text{B}^{10}(\text{Li}^6, d)\text{N}^{14}$ differential cross sections. See caption Fig. 20.

³³ V. P. Hart, E. Norbeck, and R. R. Carlson, Phys. Rev. **137**, B17 (1965).

work indicates 8.14 ± 0.04 MeV. Broad peaks corresponding to new levels at 8.54, 8.75, 8.93, 9.26, and 9.74 MeV are observed at forward angles.

Seven deuteron peaks are associated with N^{16} known energy levels in Fig. 17.

The triton spectrum in Fig. 18 is similar to the deuteron spectrum from the $B^{11}(Li^6, d)N^{15}$ reaction. A giant peak corresponding to the 9.16-MeV N^{15} state is seen. This cross section is about seven times larger than that of any other resolved level. The cross section of the 5.28-, and 5.30-MeV levels is relatively stronger than in the $B^{11}(Li^6, d)N^{15}$ reaction.

The C^{14} alpha spectrum is shown in Fig. 19. The peak labeled 10.43 may contain both levels known at 10.43 and 10.47 MeV. A small peak in Fig. 19 corresponds to 10.71 excitation energy; this peak is not apparent at many angles; however it does not result from known levels in oxygen or carbon contaminant reactions. Two peaks corresponding to 11.35 and 11.66 MeV are observed at forward angles. A reported state at 11.9 ± 0.3 MeV with $\Gamma = 1.1$ MeV is not observed. The broad peaks labeled 14.15, 14.73, and 15.07 may correspond to states

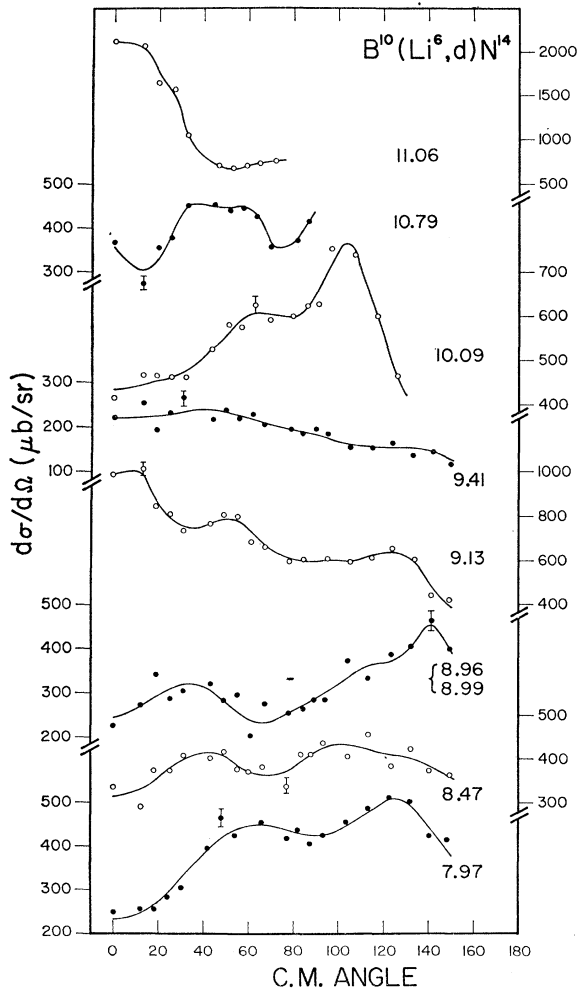


FIG. 22. $B^{10}(Li^6, d)N^{14}$ differential cross sections. See caption Fig. 20.

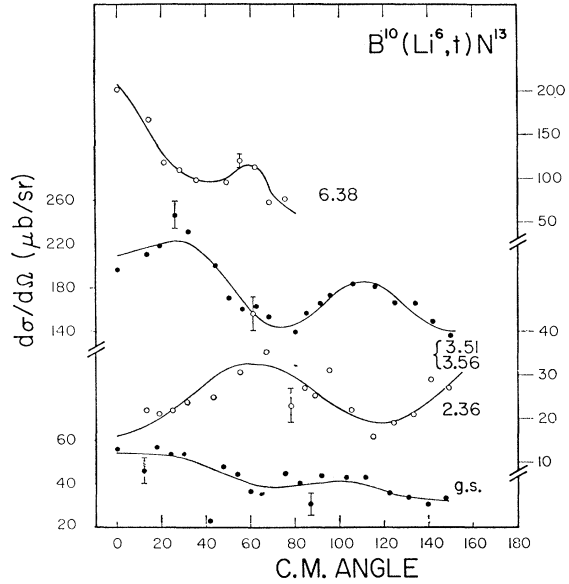


FIG. 23. $B^{10}(Li^6, t)N^{13}$ differential cross sections. See caption Fig. 20.

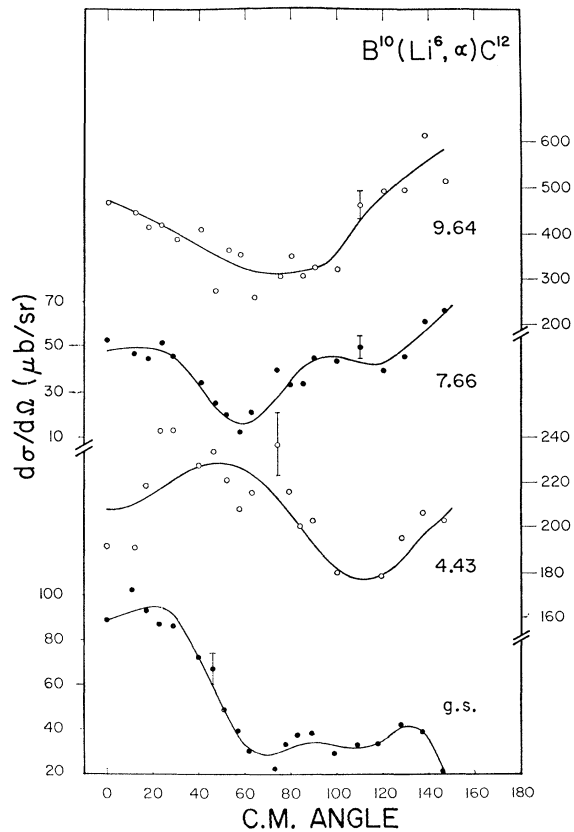


FIG. 24. $B^{10}(Li^6, \alpha)C^{12}$ differential cross sections. See caption Fig. 20.

of these excitations in C^{14} but they are not observed at enough angles to establish that they are not due to contaminants. Even without this uncertainty, it is dangerous to assign new energy levels on the basis of peaks observed on top of strong continua because final-state interactions, where multibody breakups are energetically allowed, may produce peaks in energy spectra.

IV. CROSS SECTIONS

One hundred fifteen angular distributions are shown in Figs. 20 through 38. The zero levels are suppressed in order to maximize the information content per unit figure area. The error bars for resolved groups are given by 1.25 times the standard deviation in the total number of counts. At higher excitations where a continuum background subtraction is made and/or where peaks are incompletely resolved the error bars include estimates of these extra uncertainties. No theoretical significance is attached to the lines drawn through the data points but are intended to clarify the figures. The lines represent a least mean square fit to a Legendre

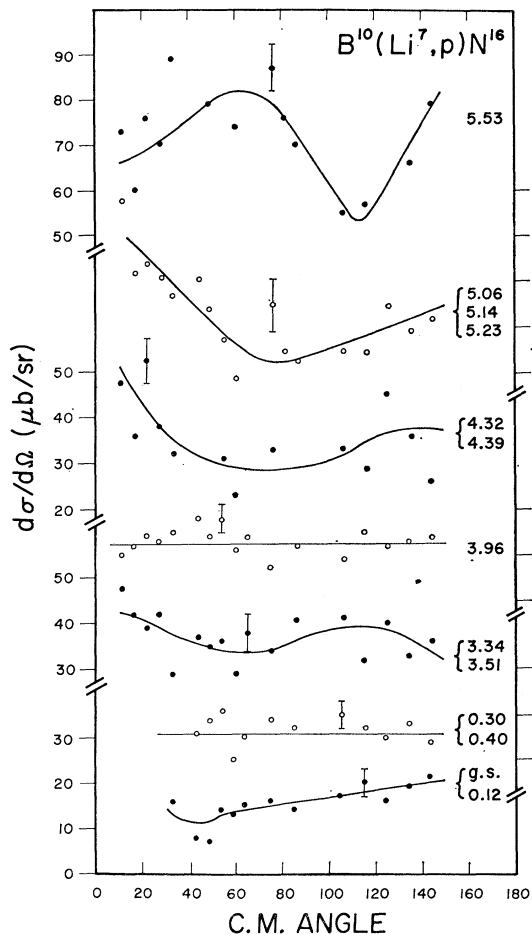


FIG. 25. $\text{B}^{10}(\text{Li}^7, p)\text{N}^{16}$ differential cross sections. See caption Fig. 20.

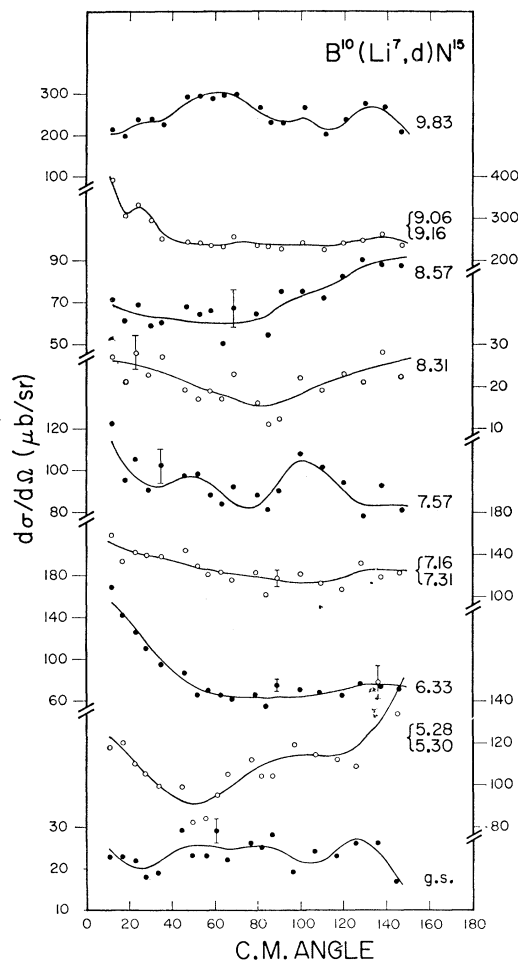


FIG. 26. $\text{B}^{10}(\text{Li}^7, d)\text{N}^{15}$ differential cross sections. See caption Fig. 20.

polynomial expansion up to P_{10} . The fitting procedure is halted when the χ^2 test indicates the probability of a worse fit is 0.05.

The differential cross sections are integrated as described above over the angular range from 0–150 deg. The 139-deg maximum laboratory angle corresponds approximately to 145 deg in the center-of-mass system. By integrating the average differential cross section over the unobserved angles, comparisons of yields are possible for some levels where the energy of the outgoing particle is too small to permit observation at many angles. The error introduced by this procedure is uncertain. Nevertheless, except for alpha particle reactions (where all the groups corresponding to the tabulated cross sections are observed at the back angles), most of the observed angular distributions have peak-to-valley ratios smaller than 2 so that the error is probably not large. The $\text{B}^{10}(\text{Li}^6, \text{He}^3)\text{C}^{13}$ cross sections are determined by data at only six forward angles (not shown). Absolute total cross sections are tabulated in Tables II through IX. Tables VIII and IX also contain lists of

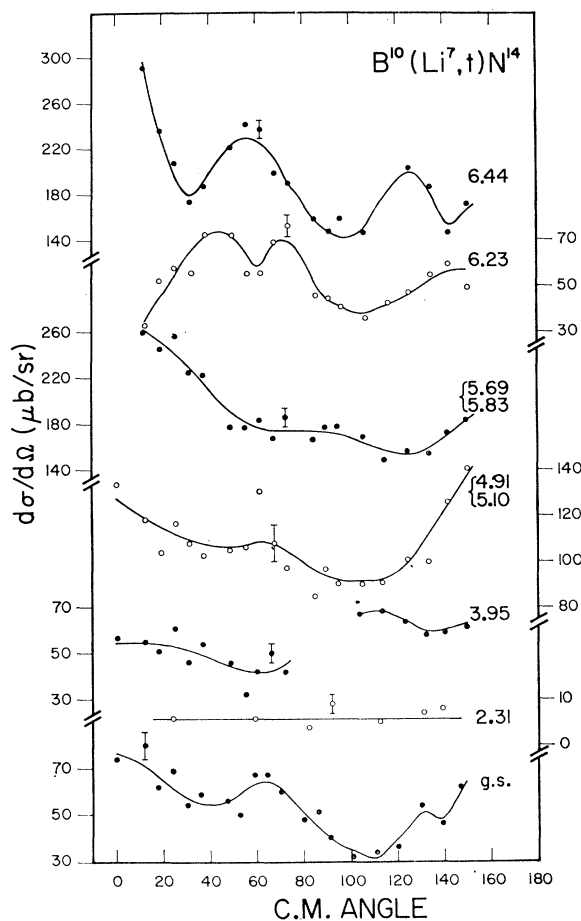


FIG. 27. $B^{10}(Li^7,t)N^{14}$ differential cross sections. See caption Fig. 20.

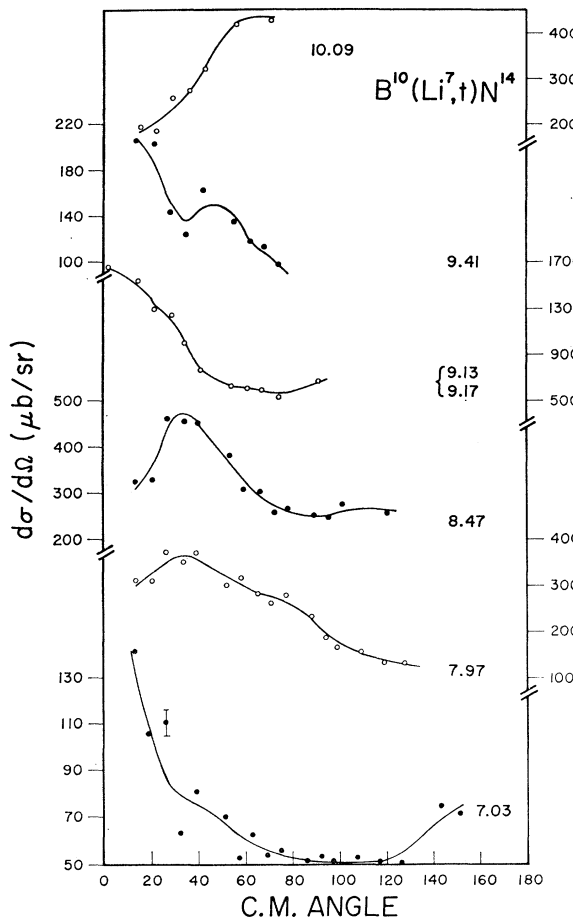


FIG. 28. $B^{10}(Li^7,t)N^{14}$ differential cross sections. See caption Fig. 20.

TABLE II. C^{12} total cross sections (mb).

Level	$J\pi^a$	$B^{10}(Li^6,\alpha)$
0.0	0+	0.50
4.43	2+	2.40
7.66	0+	0.46
9.63	3-	4.58

^a Reference 24.

TABLE III. C^{13} total cross sections (mb).

Level	$J\pi^a$	$B^{10}(Li^6,He^3)^b$	$B^{10}(Li^7,\alpha)$	$B^{11}(Li^6,\alpha)$
0.0	$\frac{1}{2}-$	0.48	0.37	0.36
3.09	+	0.42	0.20	0.23
3.68	$\frac{1}{2}-$	2.22	1.42	1.91
3.86	+			
6.86	+		1.19	1.16
7.50	$(\frac{1}{2}+)^c$		2.86	2.27
7.55	o			
7.60	+			

^a Reference 24.

^b Based on data at five angles from 0-60 deg (see text).

^c N. Nikolic, L. J. Lidofsky, and T. H. Kruse, Phys. Rev. 132, 2212 (1963).

TABLE IV. C^{14} total cross sections (mb).

Level	$J\pi^a$	$B^{11}(Li^7,\alpha)$
0.0	0+	0.20
6.09	1-	0.49
6.58	0+ ^b	
6.72	(3-)	
6.89		
7.01		
7.34	(2-)	0.66
8.32	1+	1.29

^a Reference 24.

^b E. K. Warburton, D. E. Alburger, A. Gallmann, P. Wagner, and L. F. Chase, Phys. Rev. 133, B42 (1942).

TABLE V. N^{13} total cross sections (mb).

Level	$J\pi^a$	$B^{10}(Li^6,t)$
0.0	$\frac{1}{2}-$	0.47
2.36	+	0.30
3.51	$\frac{1}{2}-$	2.02
3.56	+	
6.38	$\frac{1}{2}+$	1.21

^a Reference 24.

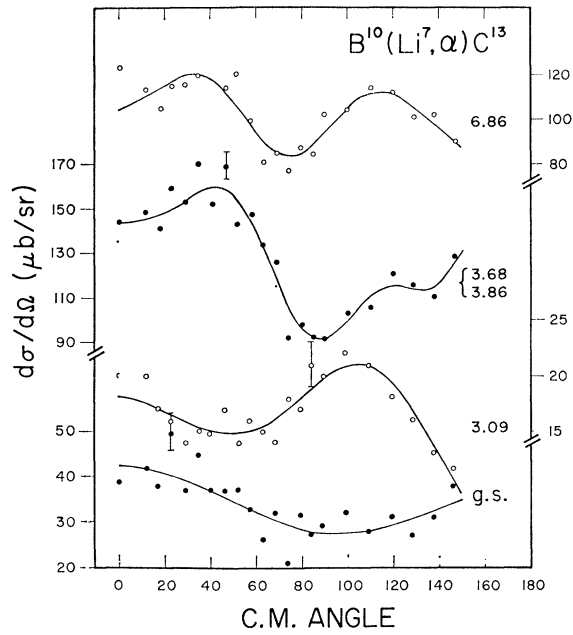


FIG. 29. $\text{B}^{10}(\text{Li}^7, \alpha)\text{C}^{13}$ differential cross sections. See caption Fig. 20.

new energy levels in N^{16} and N^{17} derived from observed proton groups in reactions 6 and 15 in Table I.

V. RESULTS

It has been argued in the Introduction that certain members of the set of reactions listed in Table I ought

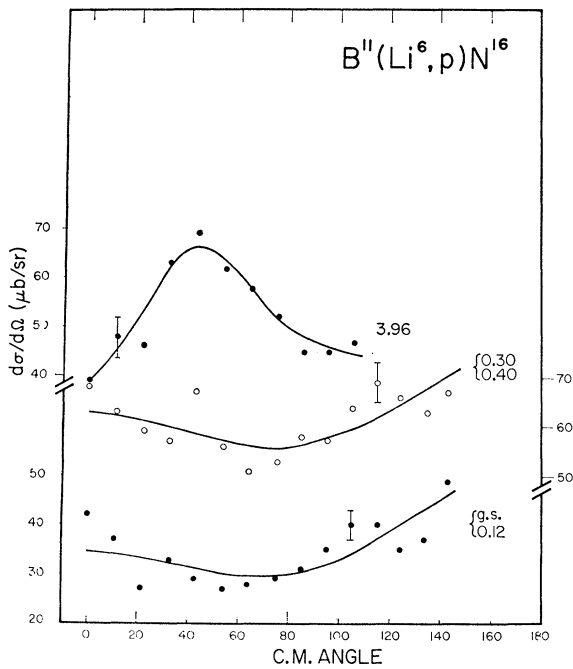


FIG. 30. $\text{B}^{11}(\text{Li}^6, p)\text{N}^{16}$ differential cross sections. See caption Fig. 20.

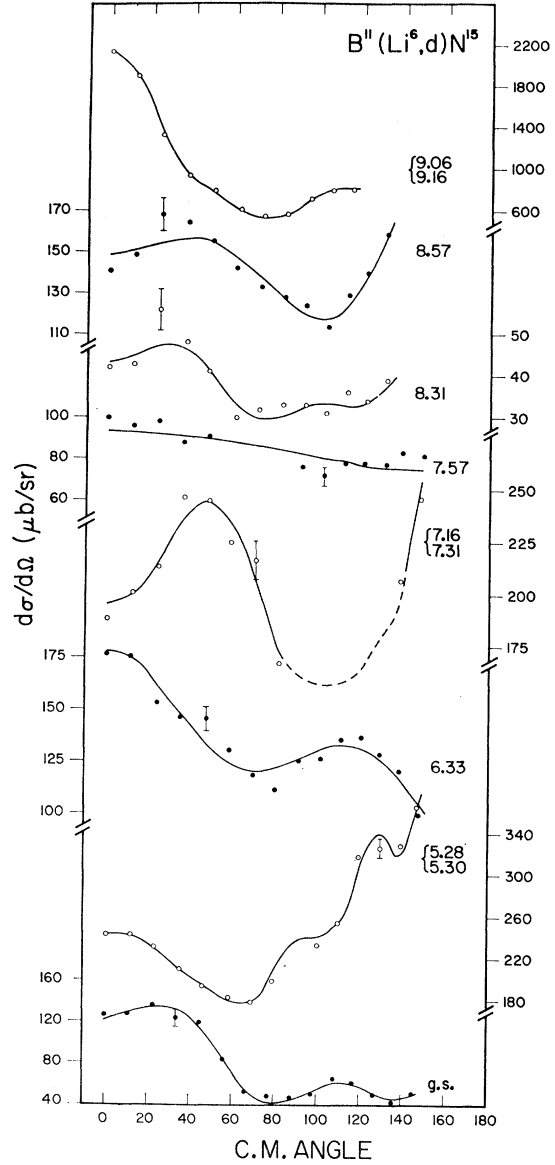


FIG. 31. $\text{B}^{11}(\text{Li}^6, d)\text{N}^{15}$ differential cross sections. See caption Fig. 20.

to have similar or dissimilar cross sections on the basis of the reaction mechanisms. For example, if direct alpha transfer is important in the (Li^6, d) , (Li^7, t) reactions, then we expect the relative cross sections of N^{14} levels in Table VI to be the same for these reactions and have no reason to expect that these will be similar to the relative cross section from the (Li^6, t) reactions. At the other extreme, if compound nucleus formation dominates the reactions, then the relative cross sections of N^{14} levels formed in the (Li^7, t) , (Li^6, t) reactions are expected to be equal if the relevant penetrabilities are not very different. Under more restrictive conditions (discussed below) the relative cross sections of N^{14} levels found in

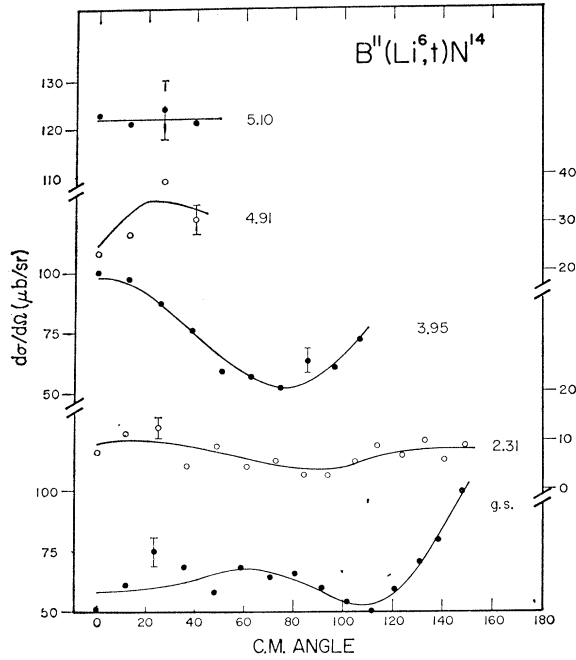


FIG. 32. $B^{11}(Li^6,t)N^{14}$ differential cross sections. See caption Fig. 20.

the (Li^6,d) should also be equal and proportional to $(2J+1)$ where J is the residual N^{14} level spin.

In fact, it can be seen from the data in Tables III, V-VIII where the same residual nucleus is formed by

TABLE VI. N^{14} total cross sections (mb).

Level	$J\pi$	T^a	$B^{10}(Li^6,d)$	$B^{10}(Li^7,t)$	$B^{11}(Li^6,t)$
0.0	1+	0	1.48	0.58	0.75
2.31	0+	1	$\leq 0.043^b$	0.078 ^c	0.080
3.95	1+	0	1.54	0.63	0.76
4.91	(0)- ^d	0	0.60	0.15 ^e	0.40
5.10	2- ^d	0	3.02	1.03	1.43
5.69	1- ^d	0	5.00	2.09	
5.83	3- ^d				
6.23	1+	0			
6.44	3+ ^f	0	1.66	0.64	
7.03	2+ ^d	0	3.83	2.17	
7.97	2-	0	1.77	0.71	
8.06	1-	1	5.05	2.87	
8.47	4-g	0	4.64	3.62	
8.71	0-	1			
8.91	3-	1			
8.96	5+g	(0)	3.73	2.27	
8.99	1+	(0)			
9.13	2-g	0	7.50	8.60	
9.17	2+	1			
9.41	1-		2.20	1.64	
10.09	(1+)	0	7.02	4.00	
10.79	h		4.64		
11.06	1+	0	10.20		
11.23	3-	1			
11.29	2-	0	5.35		

^a Except where noted, data taken from Ref. 24.

^b Based on data at six angles.

^c Based on data at seven angles.

^d Parity assignments from Ref. 27.

^e Based on data at nine angles.

^f Parity assignment from E. K. Warburton *et al.*, Phys. Rev. 134, B338 (1964).

^g Reference 28.

^h Reference 26 reports a $T=0$ level at 10.71 ± 0.09 MeV.

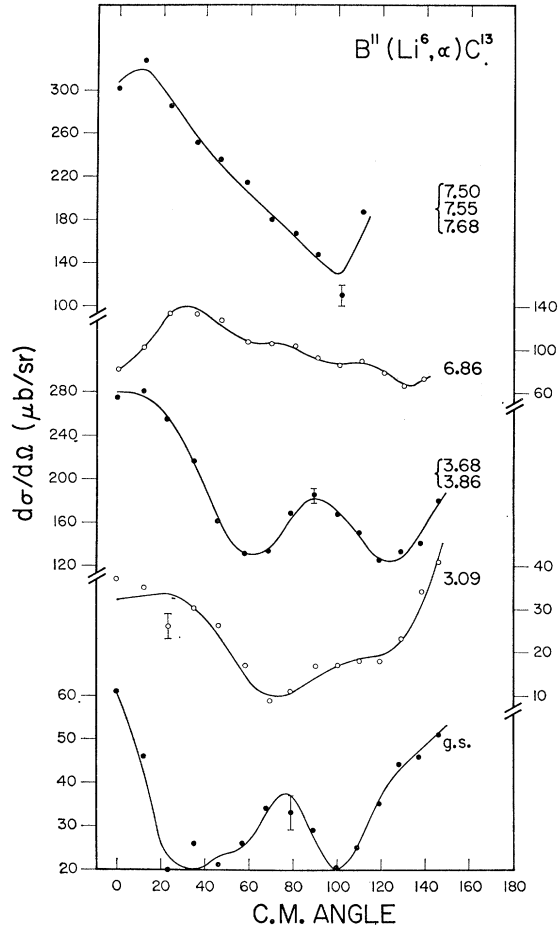


FIG. 33. $B^{11}(Li^6,\alpha)C^{13}$ differential cross sections. See caption Fig. 20.

several reactions that the relative cross sections to many low-lying residual levels are the same for different reactions. Furthermore, for levels where the spins are known these cross sections are found to be proportional to $(2J+1)$ where J is the spin of the residual level.

TABLE VII. N^{15} total cross sections (mb).

Level	$J\pi^a$	$B^{10}(Li^6,p)$	$B^{10}(Li^7,d)$	$B^{11}(Li^6,d)$	$B^{11}(Li^7,t)$
0.0	$\frac{1}{2}-$		0.28	0.80	0.59
5.28	$\frac{1}{2}+$	0.84	1.28	2.81	3.70
5.30	$\frac{3}{2}+$				
6.33	-	0.53	0.88	1.52	1.56
7.16	$\frac{1}{2}+$	0.81	1.43	2.28	2.08
7.31	$\frac{3}{2}+$				
7.57	$\frac{5}{2}+$				
8.31	$\frac{1}{2}+$, ($\frac{3}{2}+$)	0.57	1.09	0.94	1.04
8.57	$\frac{3}{2}+$	0.17	0.24	0.42	0.40
8.57	$\frac{5}{2}+$	0.40	0.83	1.62	1.84
9.06	$\frac{1}{2}+$, ($\frac{3}{2}+$)	1.71	2.91	9.15	14.30
9.16	$\frac{3}{2}-$, ($\frac{5}{2}, \frac{3}{2}+$)				
9.23	$\frac{5}{2}+$				
9.76	$\frac{1}{2}+$, ($\frac{3}{2}, \frac{5}{2}-$)				
9.83	$\frac{3}{2}+$				
9.93	$\frac{1}{2}+$, ($\frac{3}{2}, \frac{5}{2}-$)		≤ 3.20	≤ 3.7	

^a A tabulation of recent information on N^{15} is provided by E. K. Warburton, J. W. Omes, and D. E. Alburger, Phys. Rev. 140, B1202 (1965).

At higher excitations, smaller Q value, cross sections typically deviate upwards from the $(2J+1)$ proportionality established for lower levels. This effect is pronounced in several states formed by the (Li^6, d) , (Li^7, t) reactions: the 9.16-MeV, N^{15} , and 9.13-, 10.09-, and 11.06-MeV, N^{14} states. Although the experimental

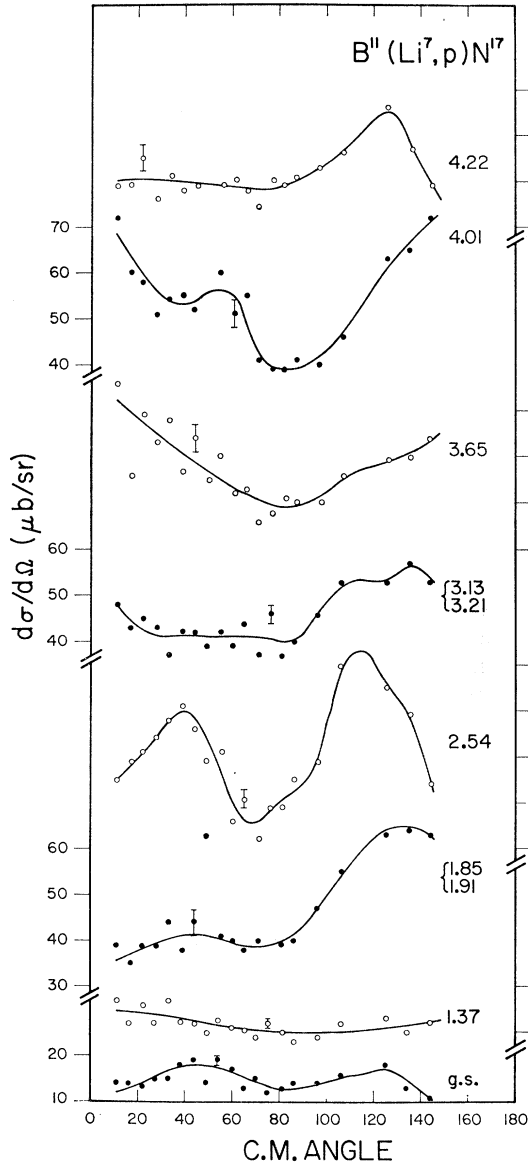


FIG. 34. $\text{B}^{11}(\text{Li}^7, p)\text{N}^{17}$ differential cross sections. See caption Fig. 20.

energy resolution (110 keV) is insufficient to resolve the 9.06-, 9.16-, 9.22-MeV, N^{15} levels, the observed peak energy and width imply the 9.16-MeV population is much the stronger of the three. The enhancement of these levels is even more obvious if the cross sections are divided by $(2J+1)$.

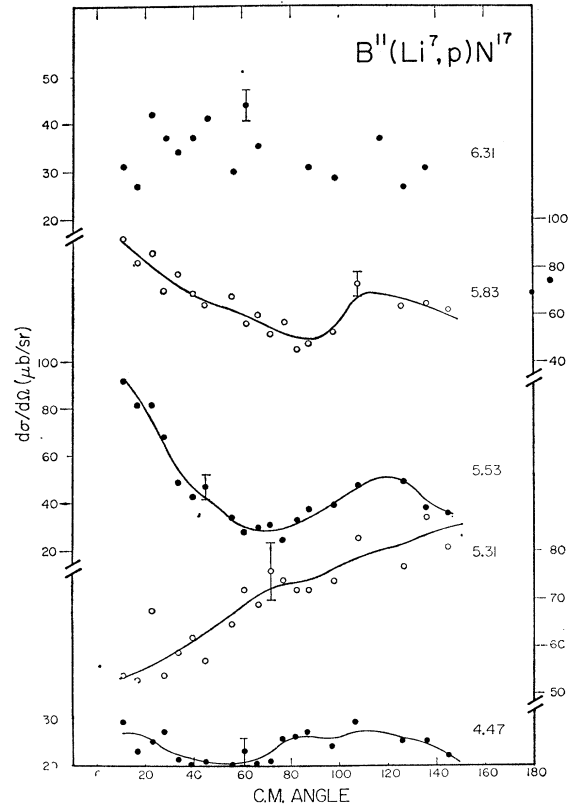


FIG. 35. $\text{B}^{11}(\text{Li}^7, p)\text{N}^{17}$ differential cross sections. See caption Fig. 20.

TABLE VIII. N^{16} total cross sections (mb).

Level	$J\pi^a$	Present work	$\text{B}^{10}(\text{Li}^7, p)$	$\text{B}^{11}(\text{Li}^6, p)$	$\text{B}^{11}(\text{Li}^7, d)$
0.000	2-				
0.120	0-		0.18	0.39	0.79
0.296	3-			0.70	1.47
0.396	1-		0.30		
3.34	1+b		0.43		0.89
3.51	(0+)b				1.05
3.96	(1-)b		0.38	0.61	1.17
4.32	(1+)		0.39	0.73	1.77
4.39	1-				
4.77		4.80±0.05			
4.88					
4.98					
5.06		5.10			
5.14					
5.23					
5.53		5.53			
5.73°		5.73			
6.29°		6.30			
6.40°		6.40			
6.55°		6.55			
		7.66			
		8.10			
		8.36			
		8.83			
		9.47			

^a Reference 24.
^b Spins, parities taken from Ref. 46.
^c Energies taken from Ref. 31.

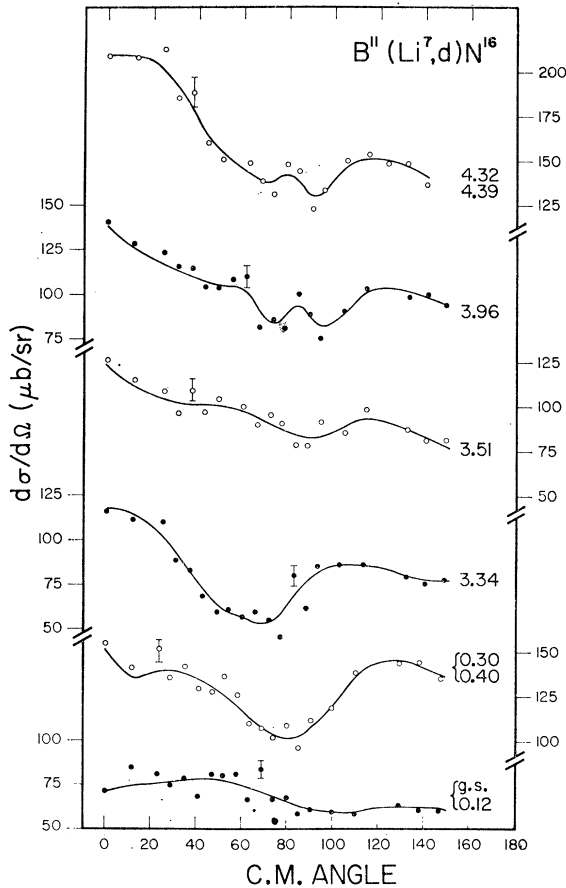


FIG. 36. $B^{11}(Li^7,d)N^{16}$ differential cross sections. See caption Fig. 20.

In general, the angular distributions shown in Figs. 21 through 38 are not symmetric about 90 deg. Often the peak-to-valley ratio is less than two. Exceptions occur in the alpha particle reactions and in the (Li^6,d) , (Li^7,t) reactions to the large yield states discussed above. In general, no similarity exists between (Li^6,d) and (Li^7,t) distributions to given final states. This implies little about the direct-reaction nature of these reactions. It has been pointed out that the allowed angular momentum transfers are different for direct alpha stripping. Furthermore, if heavy-particle stripping is important, the distributions cannot be expected to be similar.

Morrison *et al.*⁹ have measured the angular distributions of the deuteron and triton reactions from the ground and first few excited states of N^{14} and N^{15} at 4.5 MeV. The present results for N^{14} are in general different. For N^{15} the results are more similar, particularly for the (Li^6,d) and (Li^7,t) reactions. The alpha particle groups studied by Morrison⁴ at 3.5-MeV incident energy exhibit maxima and minima at approximately the same angles as found here; however the peak-to-valley ratios are different.

VI. DISCUSSION

It would seem difficult to reconcile these cross-section results to low-lying levels with a dominant direct-reaction mechanism. Expressions for direct stripping contain the $(2J+1)$ phase-space factor. Usually, however, the stripping cross sections do not exhibit this dependence because the residual level configurations, and thereby the reduced widths, vary from level to level. [In the special case of a closely spaced multiplet the reduced widths are equal, and spins have been assigned³⁴ on the basis of a $(2J+1)$ cross-section dependence.]

On the other hand, in the statistical compound

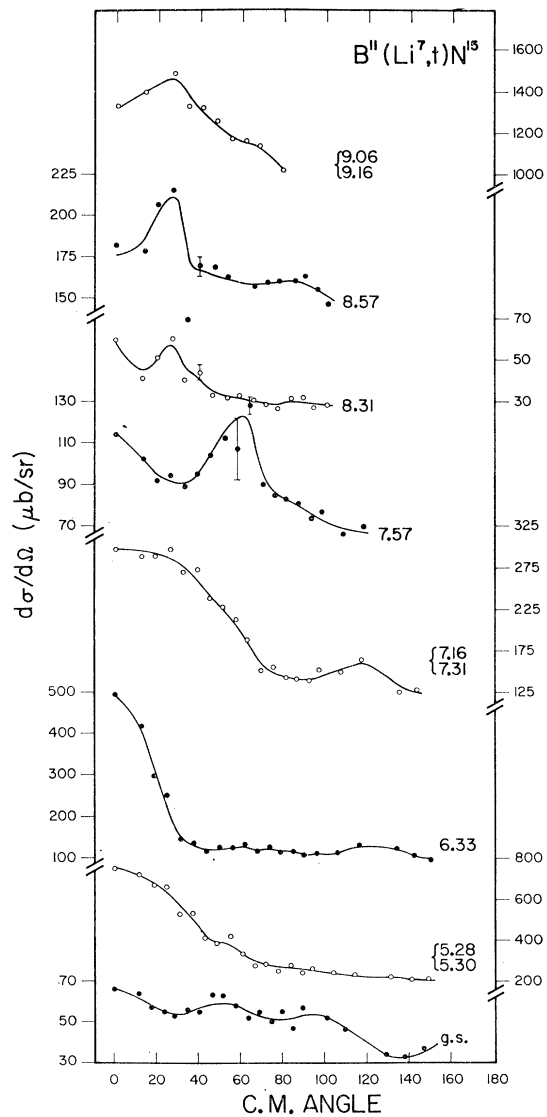


FIG. 37. $B^{11}(Li^7,t)N^{15}$ differential cross sections. See caption Fig. 20.

³⁴ H. A. Enge, Phys. Rev. **94**, 730 (1954); J. R. Erskine, W. W. Buechner, and H. A. Enge, *ibid.* **128**, 720 (1962).

nucleus theory (SCN) in which reactions proceed via a large number of intermediate compound states, correlations between initial and final states are destroyed. Relative cross sections are determined by penetrabilities and phase-space factors. The Hauser-Feshbach equation³⁵ for the angle integrated cross section of the reaction $A(a,b)B$ is

$$\sigma(a,b) = \frac{\pi}{k_a^2(2J_A+1)(2J_a+1)} \sum_{I\pi} (2I+1) \times (\sum_{s,l} T_l(E_a) \sum_{s',l'} T_{l'}(E_b) / \sum_{C''} T_{C''}(E_{C''})), \quad (1)$$

where s, s' and l, l' are initial-, final-channel spins and angular momenta and I is the spin of the compound nucleus. The sum over C'' includes all channels energetically possible. For $T_l \ll 1$. Equation (1) can be derived³⁶ from R matrix theory with

$$T_C = 4\pi P_C S_C, \quad (2)$$

where P_C and S_C are the penetrability and strength function for channel C . Vogt *et al.*³⁶ discuss the validity of Eq. (1) where $T_l \sim 1$, the case for most reactions induced by alpha or heavier particles.

The level-density formula of Newton³⁷ is used to estimate spin-zero level density, $\rho(0)$. Pairing energy corrections are taken from Cameron.³⁸ The level density

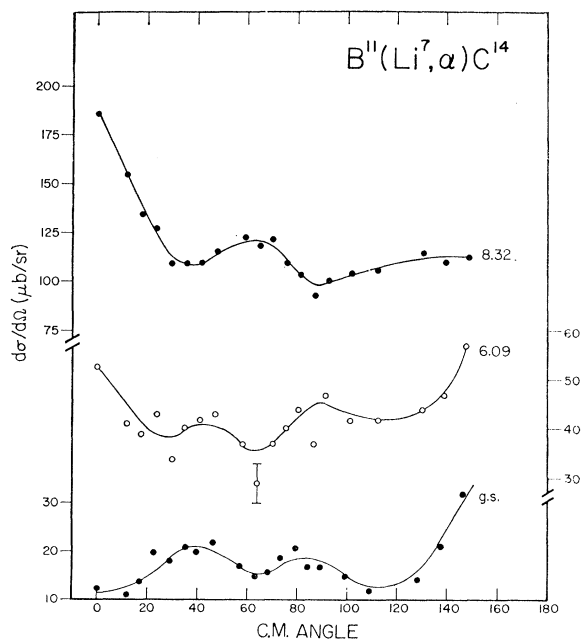


FIG. 38. $B^{11}(Li^7, \alpha)C^{14}$ differential cross sections. See caption Fig. 20.

³⁵ W. Hauser and H. Feshbach, Phys. Rev. **87**, 366 (1952).

³⁶ E. W. Vogt, D. McPherson, J. A. Kuehner, and E. Almqvist, Phys. Rev. **136**, B99 (1964).

³⁷ T. D. Newton, Can. J. Phys. **34**, 804 (1956).

³⁸ A. G. W. Cameron, Can. J. Phys. **36**, 1040 (1958).

TABLE IX. N^{17} total cross sections (mb).

Level	$J\pi^a$	Present work	$B^{11}(Li^7, p)$
0.0			0.18
1.37			0.25
1.85			0.57
1.91			
2.54			0.73
3.13			0.54
3.21			
3.65			0.42
4.01			0.56
4.22 ^b			0.27
4.47 ^b		4.47±0.04	0.28
5.21 ^b		5.23	0.84
5.53 ^b		5.51	0.50
5.83 ^b		5.83	0.73
6.07 ^b		6.09	
6.25 ^b		6.23	
6.45 ^b		6.41	
6.61 ^b		6.62	
6.99±0.03 ^b		6.99	
(7.26)±0.07 ^b		7.17	
		7.37	
(7.51)±0.07 ^b		7.63	
7.79±(0.02) ^b		7.73	
8.00±0.03 ^b		8.00	
(8.25)±0.03 ^b		8.14	
		8.55	
		8.93	
		9.26	
		9.74	

^a Reference 24.

^b Reference 33.

of spin I is then computed from

$$\rho(I) = (2I+1)\rho(0)e^{-I(I+1)/2\sigma^2},$$

where the spin cutoff parameter σ^2 is set equal to 6.¹² A lower limit of Γ , an average compound nucleus level width, can be estimated in the evaporation approximation.³⁹ For O^{17} at 30 MeV, one finds $\Gamma > 80$ keV. Table X lists the estimated center-of-mass energy loss ΔE , number of levels with $J \leq 8$ contained in ΔE , and $\Gamma\rho(0)$ where Γ is taken to be 80 keV for the reactions in Table I. These must obviously be considered crude estimates not only because of the lightness of the nuclei but also because of the high-excitation energies. It seems probable, however, that in the present work $\Delta E \sim \Gamma$, $\Gamma/D > 1$, and $\Delta E/D > 1$.

TABLE X. Estimated target center-of-mass energy losses ΔE , compound-nucleus level densities from $J=0$ through 8 (see text) and Γ/D_0 where Γ is taken as 80 keV and $D_0 = 1/\rho(0)$.

Reaction	Compound-nucleus excitation (MeV)	Target energy loss ΔE (keV)	$\sum_{J=0}^8 \rho(J)$ (MeV ⁻¹)	$\frac{\Delta E}{\sum \rho(J)}$	Γ/D_0
$Li^6 + B^{10} \rightarrow O^{16}$	33.9	50	870	62	7.2
$Li^7 + B^{10} \rightarrow O^{17}$	30.8	50	3300	160	27.0
$Li^6 + B^{11} \rightarrow O^{17}$	26.6	55	1330	73	11.0
$Li^7 + B^{11} \rightarrow O^{18}$	27.4	100	3100	310	25.0

³⁹ T. Ericson, Advan. Phys. **9**, 425 (1960).

Ericson shows⁴⁰ that the rms fluctuation in the angle integrated SCN cross section is on the order of $1/\sqrt{N}$, where N is the effective number of channels connecting a and b in the sharp cutoff approximation ($T_l = T$ for $l \leq L$, $= 0$ for $l > L$).

$$N = T^{-2} \sum_{ss'} \sum_{ll'} T_l(a) T_{l'}(b).$$

Taking $l \sim l' \leq 5$ and $s, s' \leq 2$, then $N \sim 140$. Thus rms fluctuations on the order of 8% or less are expected in the present cross sections. Ericson finds⁴⁰ that a lower limit for differential-cross-section rms fluctuations is given by

$$\frac{1}{\sqrt{N}} = \left[\frac{2}{(2J_a+1)(2J_{A+1})(2J_b+1)(2J_{b+1})} \right]^{1/2}. \quad (3)$$

For the $B^{10}(Li^6, d)N^{14}$ ground state reaction, $1/\sqrt{N} = 10\%$. It must be stressed that this is a lower limit. To summarize, it appears that SCN is applicable to this experiment with $\Gamma/D > 1$. Further the large spins and angular momenta are expected to damp the Ericson fluctuations.

MacDonald has shown¹² that under certain condi-

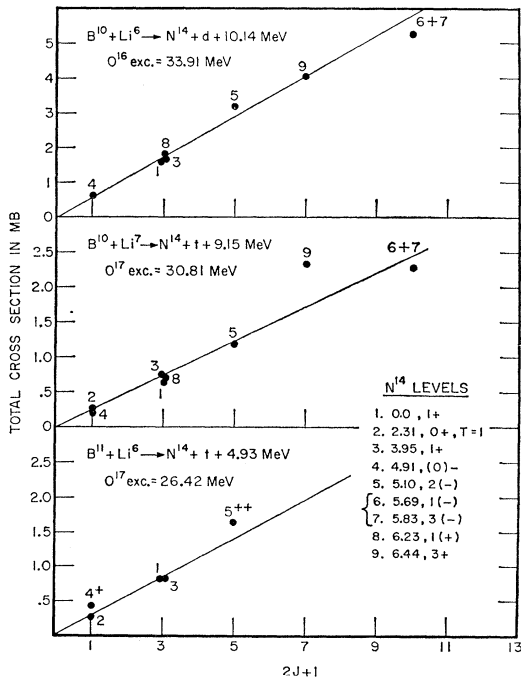


FIG. 39. N^{14} total cross section in mb versus value of $(2J+1)$. The differential cross sections are integrated and normalized to the range 0° - 150° as discussed in text. The (+) and (++) points are observed only over 0° to 40° . Level excitations are given in MeV; level data are taken from Table VI.

⁴⁰ T. Ericson, *Ann. Phys.* **23**, 390 (1963).

tions Eq. (1) predicts cross-section proportionality to $(2J+1)$. The conditions, in addition to those required by SCN, are:

- (i) Many orbital angular momenta contribute to the reaction.
- (ii) Average initial and final angular momenta $\gg J$.
- (iii) $E_i \gg E_b$, where E_i, E_b are the exit-channel energy and Coulomb barrier.

A number of papers have already reported $(2J+1)$ dependences. Most have dealt with the (n, α) reaction⁴¹ and the $Al^{27}(d, \alpha)Mg^{25}$ reactions.⁴²⁻⁴⁴ A preliminary report of the lithium-boron $(2J+1)$ dependence has been published elsewhere.⁴⁵ Some of the cross sections

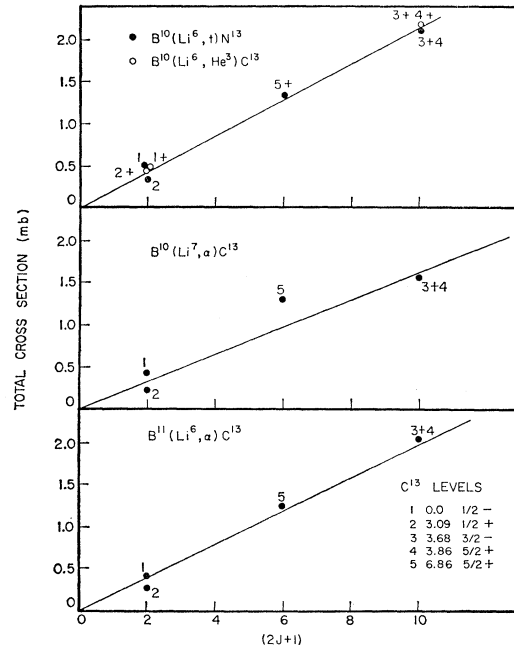


FIG. 40. N^{13}, C^{13} total cross sections in mb versus $(2J+1)$. The (+) points are observed only over 0° to 60° . Level data taken from Tables III and V.

listed in Tables II through IX are plotted versus $(2J+1)$ in Figs. 39 through 41.

Consider N^{14} : It is observed via three different reactions. The total cross sections for low-lying levels are plotted versus $(2J+1)$ in Fig. 39. The 2.31-MeV

⁴¹ L. Colli, I. Iori, M. G. Marazzau, and M. Milazzo, *Nucl. Phys.* **43**, 529 (1963).

⁴² S. Hinds, R. Middleton, and A. E. Litherland, in *Proceedings of the Rutherford Jubilee Conference*, edited by J. Birks (Academic Press Inc., New York, 1961), p. 305.

⁴³ O. Hansen, E. Koltay, N. Lund, and B. S. Madsen, *Nucl. Phys.* **51**, 307 (1964).

⁴⁴ I. M. Naqib, R. Gleyvod, and N. P. Heydenburg, *Nucl. Phys.* **66**, 129 (1965).

⁴⁵ R. R. Carlson and R. L. McGrath, *Phys. Rev. Letters* **15**, 173 (1965).

0+, T=1 level cross section is not plotted for the B¹⁰(Li⁶,d)N¹⁴ reaction because it is forbidden by isotopic spin selection rules. The yield to this state in the B¹⁰(Li⁷,t)N¹⁴ and B¹¹(Li⁶,t)N¹⁴ reactions is multiplied by 3 in order that the yield can be compared with the T=0 data. The initial systems have T=1/2, T₃=1/2 with the final system consisting of N¹⁴ with T=1, T₃=0 and a triton with T=1/2, T₃=1/2 giving a factor (1/2 1 1/2 0 | 1/2 1/2)² = 1/3 in the cross section. It is clear that the low yield to this state can result from this (2T+1)⁻¹ factor and the low value of (2J+1) and not necessarily from a direct-reaction mechanism which forbids the coupling of an alpha particle to the 3+ B¹⁰ ground state to form a 0+ final state. Morrison has suggested⁸ that the negligible

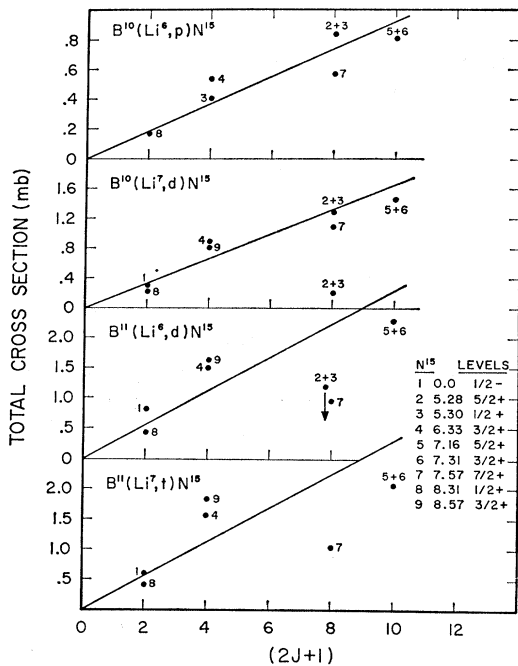


FIG. 41. N¹⁵ total cross sections in mb versus (2J+1). Level data taken from Table VII.

cross section for formation of the 1.74-MeV 0+, T=1 B¹⁰ state in the Li⁶(Li⁷,t)B¹⁰ reaction at 2-MeV bombarding energy may be due to the impossibility of coupling an alpha particle to the 1+ Li⁶ ground state to form the B¹⁰ state. It was previously mentioned that the other T=1 levels at 8.06, 8.63, 8.71 MeV are not observed above background in the B¹⁰(Li⁷,t)N¹⁴ reaction. This is to be expected. A direct capture of a T=0 alpha by the T=0 B¹⁰ cannot produce T=1 states; on the other hand, the statistical model weights these states by the factor (2T+1)⁻¹(2J+1). For example, this factor weights the 8.71-MeV 0-, T=1 state by 1/27 compared to the 8.47-MeV -4, T=0 state.

Figures 40 and 41 contain (2J+1) plots of data from other residual nuclei with known spins: N¹³, C¹³, and

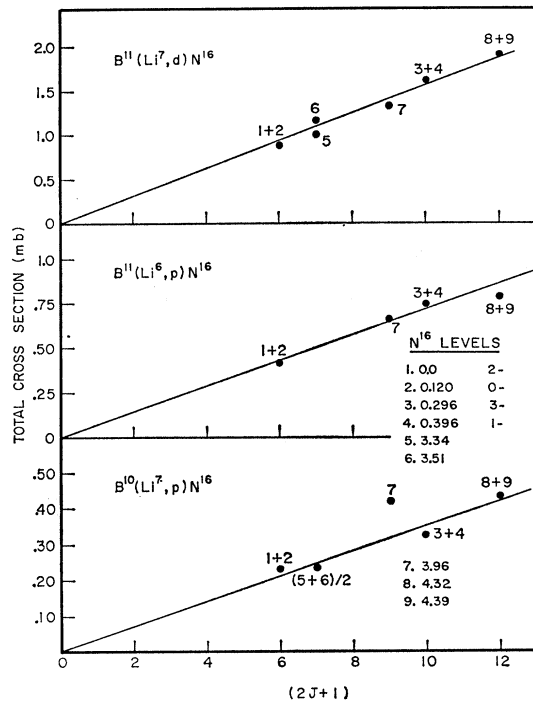


FIG. 42. N¹⁶ total cross sections in mb versus tentative (2J+1) values. Points are plotted for best (2J+1) dependence. Level data taken from Table VIII.

N¹⁵. Where unresolved doublets occur, the yield is plotted versus the sum of (2J+1) for both states. The mirror reactions B¹⁰(Li⁶,t)N¹³ and B¹⁰(Li⁶,He³)C¹³ are plotted together. Considering the large uncertainty associated with the He³ total cross sections (the integration range is less than 0 to 70 deg), the small deviations from the (2J+1) dependence are surprising.

In Fig. 41, the relationship between cross sections and (2J+1) is much better with the B¹⁰(Li⁶,p)N¹⁵ and B¹⁰(Li⁷,d)N¹⁵ reactions than with the B¹¹(Li⁶,d)N¹⁵, B¹¹(Li⁷,t)N¹⁵ reactions. The relative cross sections of these last two reactions, while deviating rather strongly from (2J+1) proportionality, are quite similar.

Table II shows that the first three C¹² levels are populated in the ratios 1:4.8:0.92, very close to the (2J+1) ratios 1:5:1. The first two C¹⁴ levels are populated in the ratios 1:2.5 which is close to the 1:3(2J+1) ratio.

The decision as to when to stop plotting levels on these graphs, as the excitation energy increases, is arbitrary. It has been remarked that highly excited levels often have very big yields. About 15% of the 67 points included in this discussion are "bad" in the sense that if the spin were not known *a priori*, the wrong assignment would be made on the basis of the (2J+1) rule.

In spite of this, it is tempting to assign tentative spins of levels in N¹⁶ and N¹⁷ from the total cross sections. Figure 42 shows three reactions leading to N¹⁶.

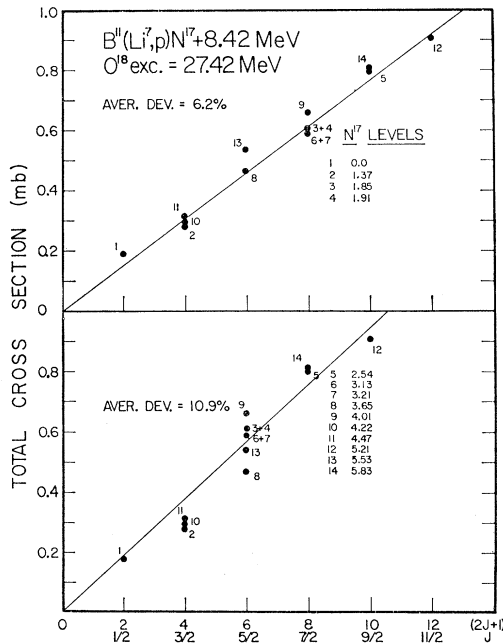


FIG. 43. N^{17} total cross sections in mb versus tentative $(2J+1)$ values. The arrangement in the upper part of the figure gives smallest average deviation but is inconsistent with other data; lower arrangement is more consistent with other data (see text). Level data taken from Table IX.

The spins of the four low-lying states of this nucleus are known. These points define a line which passes through the origin in each case. In addition, the relative yields of the three reactions are consistent [with the exception of the $B^{10}(Li^7,p)N^{16}$ 3.96-MeV reaction]. Nevertheless, the extrapolation from several hundred-keV to about 3.5-MeV excitation energy is unreliable since it has already been observed that at some point, as the level excitation is increased, the yields to levels with known spins lose the $(2J+1)$ proportionality. The sum of yields to the 3.34–3.51 states corresponds to $(2J_1+1)+(2J_2+1)=14$; implying the spins to these states are either 0, 6; 1, 5; 2, 4; or 3, 3. The 3.96-MeV state is assigned spin 4. The two states at 4.32, 4.39 may have spins 0, 5; 1, 4; or 2, 3. These spin assignments do not agree with spins deduced from $N^{15}+n$ total-cross-section measurements by Fossan *et al.*⁴⁶ 3.34 MeV, 1+; 3.51, (0+); 3.97, (1-); 4.32, (1+); 4.39, 1-.

The ground-state spin of N^{17} is $\frac{1}{2}$ -.⁴⁷ No other spins are known. Gamma-ray branching ratios have been measured by Hart *et al.*³³ in this laboratory via the Li^7+B^{11} reaction. Plots of the cross sections versus $(2J+1)$ are shown in Fig. 43. The average deviations

about the least mean squares fits are 6.2 and 10.9%. The former fit must be rejected since these spin assignments imply several gamma-ray transitions with 3 and 4 units of angular momentum change. The second set is consistent with the data of Hart *et al.*, except for the 2.54-MeV state; a spin assignment $\frac{7}{2}$ implies at least an $E3$ transition for the observed gamma decay to the ground state. Clearly the same reservation must be attached to spin assignments here as for N^{16} . No calibration points with large excitation energy and/or large spin are known for these nuclei so that spin assignments are speculative.

Deviations from the $(2J+1)$ dependence occur as the level excitation increases. Usually the cross sections are larger, not smaller, than given by the $(2J+1)$ proportionality established for lower levels. The opposite situation is expected in the SCN picture because smaller exit penetrabilities correspond to the higher excitations. Instead the deviations may be due to increased direct-reaction contributions which supplement the SCN process. Two aspects of these reactions may act to attenuate direct-reaction mechanisms for large Q values. Consider direct alpha transfer in the (Li^6,d) reactions. If the α - d interaction is responsible for the momentum transfer to the deuteron, then it follows that the α - d system must have on the order of 12-MeV vibrational energy for the ground-state reactions. For reactions near zero Q the required vibration energy is only about 1 MeV. Inglis⁴⁸ has pointed out that vibrational energies much larger than the binding energies of $(\alpha+d)$ or $(\alpha+t)$ systems (1.47) and 2.47 MeV) are suppressed if the cluster-model description is valid. A general feature of the reactions in this experiment is that the momentum transfers to the outgoing particles are large for ground-state reactions.

The second characteristic of these reactions is the rather complicated cluster of nucleons to be transferred in a direct interaction. Low-lying levels of light nuclei are often well described by one- or two-particle or hole excitations. In coupling, say, an alpha particle to B^{11} to form N^{15} levels, the four nucleons must in general be inserted into different shell-model orbits. The nucleons are not well correlated in space and probably do not have large overlap with the alpha particle. At higher excitations states exist where more nucleons can be inserted into equivalent shells so that the overlaps can become larger. In other language, cluster states are expected to exist near cluster thresholds.² The large yield of the 9.16-MeV N^{15} and 11.06-MeV (along with the 9.13- and 10.09-MeV) N^{14} states in the (Li^6,d) and (Li^7,t) reactions perhaps indicates that they are states of this type. From

⁴⁶ D. B. Fossan, R. A. Chalmers, L. F. Chase, and S. R. Salisbury, Phys. Rev. **135**, B1347 (1964).

⁴⁷ M. G. Silbert and J. C. Hopkins, Phys. Rev. **134**, B16 (1964).

⁴⁸ D. R. Inglis, Phys. Rev. **126**, 1789 (1962).

TABLE XI. Total cross sections (mb) $\div (2J+1)$. Numbers are derived from slopes of lines in Figs. 39 through 43 and from cross-section data on first three C^{12} and C^{14} levels in Tables II and IV.

	Protons	Deuterons	Tritons	Alphas
$\text{Li}^6 + \text{B}^{10}$	0.085	0.55	0.20	0.50
$\text{Li}^7 + \text{B}^{10}$	0.035	0.15	0.25	0.15
$\text{Li}^6 + \text{B}^{11}$	0.070	0.35	0.25	0.20
$\text{Li}^7 + \text{B}^{11}$	0.075 or 0.094	0.16	0.30	0.20

Table VII it is clear that this N^{15} state is populated more strongly by these reactions than by (Li^6, p) or (Li^7, d) reactions. Unfortunately the N^{14} states are not observed in other kinds of reactions.

We note that the $\frac{3}{2}^-$ spin parity of the N^{15} level is consistent with coupling an $L=0$ alpha particle to B^{11} . This is equivalent to the $(1s)^4 p^7 (2s)^4$ shell-model configuration; however, the $s^4 p^7 (2s, 1d)^4$ or $s^4 p^9 (2s, 1d)^2$ configurations might give $\frac{3}{2}^-$ spin, parity also. None of the large yield 11.06-, 10.09-, or 9.13-MeV N^{14} states are $3+$, the spin-parity resulting from coupling a B^{10} to an $L=0$ alpha. The (Li^6, d) angular distributions leading to the 9.16-MeV N^{15} and 11.06-MeV N^{14} states are suggestive of a direct alpha transfer mechanism in the sense that both peak more strongly in the forward direction than the other reactions.

To summarize, it has been suggested that the observed $(2J+1)$ dependence reflects the importance of the SCN mechanism, and that enhanced yields as the Q decreases can be attributed to increasingly important direct-reaction processes.

Several objections arise. First, the onset of direct-interaction processes is not very well defined with respect to the Q value. For example, the alpha particle reactions deviate from $(2J+1)$ dependence at much larger Q ($Q \geq 12$ MeV) than reactions involving the emission of other particles (in some cases $Q \sim 0$). Also Morrison's⁴ alpha particle angular distributions at 3.5 MeV are similar to those obtained here. Both the $(2J+1)$ deviations and the constancy of the angular distributions are taken to imply that direct-reaction processes contribute significantly to these cross sections.

Second, the (Li^6, d) , (Li^7, t) reactions leading to N^{15} levels exhibit poor $(2J+1)$ dependence for some low-lying levels and particularly for the 5.28–5.30 MeV doublet. It has been pointed out that the angular distributions of Morrison *et al.*⁹ at 4.5 MeV are similar to the present results for the (Li^6, d) , (Li^7, t) reactions leading to the four lowest N^{15} levels. On the other hand, the distributions leading to N^{14} levels do not have the same appearance at 4.5 MeV.⁹ This may imply relatively stronger direct-reaction contributions to the N^{15} states and hence is consistent with the observed lack of $(2J+1)$ proportionality.

Finally, if the strength functions defined by Eq. (2) do not change over the excitation shift from 30.8 to 26.6 MeV in O^{17} , then the SCN theory implies that the cross-section ratios to given final states formed in the $\text{Li}^7 + \text{B}^{10}$ and $\text{Li}^6 + \text{B}^{11}$ reactions should be less than unity. Table XI shows the slopes of the $(2J+1)$ lines given in Figs. 39 through 43. The slopes determined by the first few C^{12} and C^{14} levels are also given. The ratio of slopes of various particle groups from the $\text{Li}^7 + \text{B}^{10}$ and $\text{Li}^6 + \text{B}^{11}$ reactions are not constant, but are less than unity except for the triton reactions. It is interesting that from Table XI, the slopes are such that: $(\text{Li}^6, d) > (\text{Li}^6, t)$, and $(\text{Li}^7, t) > (\text{Li}^7, d)$. Provided the strength functions do not vary in a fortuitous manner, it appears that the enhancement of cross sections involving the emission of clusters existing in the lithium nuclei may be in disagreement with the SCN assumptions. The basic assumption is, of course, that the compound nucleus lifetime is long enough to establish equilibrium. However Table I shows, with the exception of $\text{Li}^7 + \text{B}^{10}$, that the dependence of exit channel penetrabilities on Q -value might also produce these results.

VII. CONCLUSION

The relative cross sections of many of the low-lying levels formed in the lithium-boron reactions are found to be closely proportional to $(2J+1)$. Cross sections for the formation of lower Q , residual levels at higher excitations, are on the average larger. The extent of the deviations varies for different reactions.

It has been assumed that direct-reaction mechanisms do not give $(2J+1)$ cross-section dependences because of fluctuating reduced widths. The statistical compound nucleus theory (SCN) can be expected to lead to the observed $(2J+1)$ dependences. It is thus suggested that this process dominates the reactions to low-lying levels; however, we have pointed out that the slopes of the $(2J+1)$ lines imply that equilibrium may not be established at these high compounds nucleus excitations and hence the $(2J+1)$ dependence may arise in part from the $(2J+1)$ phase-space factor in direct reactions. Direct-reaction mechanisms certainly do contribute to the cross sections for low Q or high-excited states.

The alpha particle reactions tend to deviate from $(2J+1)$ at larger Q 's than other reactions. This result, together with the similarity of the alpha angular distributions measured here with those of Morrison at 3.5 MeV,⁴ implies that direct-reaction mechanisms are important in these cases. This conclusion is in agreement with the $\text{Li}^6 + \text{C}^{12}$ work.^{6,7} On the same evidence it is concluded that direct-reaction processes are relatively stronger in the (Li^6, d) and (Li^7, t) reactions leading to N^{15} than in the same reactions leading to N^{14} .

The statistical-model cross sections are expected to peak near the Coulomb barrier [the experimental results and Hauser-Feshbach calculations show this very

nically for the $Al^{27}(d,\alpha)Mg^{25}$ reaction⁴⁹]. Thus, compound nucleus contributions are maximized at the lithium energies in this experiment. In addition, the large angular momenta ($L < 5\hbar$) carried in by the heavy projectiles, and the large Q values are prerequisites¹² for the SCN ($2J+1$) dependence. Therefore reactions like those studied here may be useful in establishing the domain of validity of the ($2J+1$) rule.

⁴⁹ Y. Cassagnou, I. Iori, C. Levi, T. Mayer-Kuckuk, M. Mermaz, and L. Papineau, *Phys. Letters* **7**, 147 (1963).

ACKNOWLEDGMENTS

The author expresses his appreciation to Professor R. R. Carlson for advice during the course of this work, and for writing many of the required computer analysis programs. Discussions with Professor R. T. Carpenter, Professor E. Norbeck, and Dr. D. Heikkinen have been helpful. W. Seale, M. J. Throop, and K. Kibler rendered great assistance during long data runs.

Generalized Seniority and the Surface Delta Interaction*

R. ARVIEU† AND S. A. MOSZKOWSKI
University of California, Los Angeles, California
 (Received 17 December 1965)

It is shown that the surface delta interaction (SDI), which can be defined as a delta interaction $\delta(\Omega_{12})$ in the *angles* of the interacting particles (with the additional assumption that all radial integrals are equal), provides a very simple coupling scheme for configurations of identical particles (i.e., maximum isospin) involving degenerate mixed orbits. This scheme, a generalization of the well-known seniority scheme, can be conveniently expressed in terms of "quasispin." It is shown that the SDI is a sum of a term which is a scalar with respect to quasispins and a term which is proportional to the number of particles. The well-known pairing interaction, like the SDI, is diagonal with respect to quasispin but is not a quasispin scalar. Thus for configurations of an even number of identical particles in mixed degenerate orbits coupled by an SDI, the ground-state energy of the seniority zero ground state varies linearly with the number of particles. We can also apply the BCS method and express the excited states in terms of quasiparticle configurations. For identical nucleons in degenerate orbits coupled by an SDI, we obtain the exact energies of the ground-state and low-lying levels.

I. INTRODUCTION

THE seniority scheme¹ has been very helpful for the interpretation of spectra involving identical particles, e.g., neutrons, in partially filled orbits. As is well known, *any* interaction conserves seniority for states in a single subshell of angular momentum $j \leq \frac{7}{2}$. For $j \geq \frac{9}{2}$, seniority is not, in general a good quantum number, even in pure j - j coupling, except for simple interactions, such as pairing, delta, or odd tensor interactions. However, for nuclei where the $g_{9/2}$ shell is filling, it has been found that reasonable effective interactions^{2,3} lead to only a very slight breakdown of seniority in the wave functions.

The seniority scheme can be generalized in one of two ways: First, we may allow both neutrons and protons to occupy a given j shell. (In this case the symmetry involved is frequently called symplectic symmetry.⁴)

However, it has been found⁵ empirically that even for $j = \frac{7}{2}$ the effective interaction does not preserve that type of symmetry even approximately. In particular, symplectic symmetry is violated by a charge-independent δ interaction but is preserved by a pairing interaction⁶; which acts between np pairs as well as nn and pp pairs (when they couple to $J=0$). Our paper will deal exclusively with the second possible generalization of seniority—its extension to systems of identical particles filling several subshells.

Here, the quasispin technique⁷⁻¹⁰ has provided a very useful tool to deal with seniority and its generalization to mixed orbitals. Quasispin has been used, for example, by Kerman and by Lawson and MacFarlane to carry out an exact diagonalization with a pairing force. When the single-particle orbits involved are all degenerate, the states are eigenfunctions of a quasispin and of a generalized seniority. However, this simplification might

* This work was supported in part by the National Science Foundation.

† Permanent address: Laboratoire de Physique Theorique, Orsay, Seine-et-Oise, France.

¹ G. Racah, *Phys. Rev.* **63**, 367 (1943).

² I. Talmi and J. Unna, *Nucl. Phys.* **19**, 225 (1960).

³ S. Cohen, R. D. Lawson, and M. H. MacFarlane, *Phys. Letters* **10**, 195 (1964).

⁴ B. H. Flowers, *Proc. Roy. Soc. (London)* **A245**, 128 (1958).

⁵ J. N. Ginocchio, *Nucl. Phys.* **63**, 449 (1965).

⁶ K. T. Hecht, *Phys. Rev.* **139**, B794 (1965).

⁷ P. W. Anderson, *Phys. Rev.* **112**, 1900 (1958).

⁸ A. K. Kerman, *Ann. Phys. (N. Y.)* **12**, 300 (1961).

⁹ K. Helmers, *Nucl. Phys.* **23**, 594 (1961).

¹⁰ R. D. Lawson and M. H. MacFarlane, *Nucl. Phys.* **66**, 80 (1965).



(a)



(b)

FIG. 2. (a) This photograph shows condensed $60 \times 128 dE/dx, E$ contour display of $p, d, t,$ and α particles from the $\text{Li}^7 + \text{B}^{11}$ reactions. (b) This photograph shows the same data after multiplication. The y axis $[dE/dx(E+E_0)]$ is shown full scale but the 1024-channel x axis (E) is condensed to 128 channels. A light pen mark is visible between the d and t groups.